1

Crystallographic Shear and Non-stoicheiometry

BY J. S. ANDERSON AND R. J. D. TILLEY

1 Introduction

When the previous Report in this series was written, detailed experimental evidence about the microstructure of crystallographic shear structures (CS phases) was just becoming available. Two themes were therefore emphasized. The first was the relation between the concept of crystallographic shear and existing views of defects and non-stoicheiometry in inorganic compounds. Most CS phases do not appear to contain point defects in significant concentrations—*i.e.* in sufficient number to contribute materially to the apparent composition ranges of CS compounds. In a heuristic sense, at least, the collapse of the parent crystal structure which produces a CS plane eliminates point defects; it is not implied that the presence of point defects in high concentration is a necessary precursor stage in the formation of a CS plane. The mechanism of this transformation process is still not clear, and the role of point defects in certain structural types, notably the 'block' structure oxides, has continued to excite interest.

A second topic, which has also been actively pursued in the review period, was the importance of coherent intergrowth between structures that are topologically compatible, but of different composition, exhibited particularly by the CS phases. It was shown that in many macroscopically homogeneous CS phases there may be a considerable measure of internal disorder, associated with irregularities in the spacing between parallel CS planes. Even though this state may not represent a true equilibrium structure, it may be experimentally inescapable and it provides a basis for apparent non-stoicheiometric properties at the macroscopic level. The usual methods of characterization and structure analysis may fail to reveal and analyse such microscopic heterogeneity; to do so needs methods for determining the local microstructure, at the unit-cell level, as distinct from the averaged structure derived from diffraction methods and from postulated models for defect structures. Such methods were beginning to emerge from the application of electron microscopy.

In the intervening two years, the power of lattice-imaging methods in electron microscopy has developed markedly. Considerable attention has been devoted to coherent intergrowth (Wadsley defects) and other forms of faulting, as observed at or below the unit-cell level, and the topological

constraints and relationships that determine the possibilities of intergrowth or structural relaxation in CS phases have been analysed. This advance in our knowledge of structure has not been matched by advances in knowledge of transport and reaction processes, and the physical properties associated with CS structures have received little study. In this review, we consider particularly the increasingly important role of electron microscopy, and the way in which structure adjusts itself to composition, both in materials that simulate non-stoicheiometric behaviour and those that are genuinely variable in composition. Crystallographic shear—the term has a very specific meaning, which should not be loosely used—is not the only transformation whereby inorganic structures can accommodate changes in the atomic ratio of metal : non-metal so as to maintain some high degree of order. Recent work has drawn attention to the formation of ordered structures, with large repeating units, where randomized solid solutions might be expected. Without venturing an answer to the difficult questions of how a solid compound should now be defined, or how complex ordering is established, we summarize also some recent developments in this wider field.

2 The Direct Observation of Structure in Crystals: Lattice Imaging

The newer experimental findings about CS phases have come largely from transmission electron microscopy and electron diffraction, rather than from *X*-ray diffraction, which has limitations imposed by the large unit cells, by the small differences in structure between one member and another in a homologous series, and, above all, by disorder in the crystals. The first results accruing from electron microscopy[1] indicated that complete order in crystals of CS phases was rarely attained; it may, indeed, be impossible even by the most careful preparative methods to obtain perfectly ordered crystals of many CS compounds for structure determination by single-crystal methods.

Transmission electron microscopy can present the essentials of the structure of CS phases and other suitable classes of compound very directly, although detailed metrical information—*e.g.* interatomic distances—cannot be extracted. For this, there is no alternative to precise structure determination by *X*-ray or, increasingly and for some purposes advantageously, neutron-diffraction methods. Lattice images can now be obtained, however, which show the projected structure at the level of the individual co-ordination polyhedron in oxide structures. Development of the technique has been largely pragmatic, based on the experimental finding that, provided that the crystals under examination were extremely thin, the contrast in micrographs made at 'optimum under-focus' approximated closely to a projection of the

[1] J. S. Anderson, 'Surface and Defect Properties of Solids', ed. M. W. Roberts and J. M. Thomas (Specialist Periodical Reports), The Chemical Society, London, 1972, Vol. 1, p. 1.

potential distribution in the crystal.[2] Thus, for CS phases, in which the density of heavy cations, of high charge, is considerably higher in the CS planes than in the relatively open matrix of parent structure, the CS planes appear as fringes which collapse into dark lines of contrast when the crystal is so oriented as to bring the CS planes parallel to the incident beam. At the highest lattice resolution, individual corner-sharing (MO_6) octahedral groups appear darker than the empty voids between them.

Interpretation of these lattice images is, however, not as straightforward as might appear at first sight. Ideally, an electron micrograph should be compared, point for point, with the intensity of the transmitted electron beam, as calculated from dynamical scattering theory. In practice, the theory of an electron-microscope image formed by the operation of many diffracted beams has been developed only in parallel with the experimental applications. Most results on CS and other structures have relied upon a less rigorous comparison with electron optic theory; much of the interpretation has, indeed, come from chemical intuition regarding the structural geometry that might be expected in the system concerned.

The correspondence between lattice images and the structures postulated from a combination of *X*-ray structural information with chemical intuition has been remarkably good, and the validity of the interpretations has not been in serious doubt. This success has stemmed from careful selection of crystalline systems, with a known basic structure, that were appropriate for attack by microscopy. The electron-microscope image could then be so focused as to give optimum contrast and resolution which brought out structural features that harmonized with expectations based on the prior knowledge of the system. Aperiodic features of the image, faulting, disorder, *etc.* could then be interpreted in a manner consistent with the interpretation in perfect regions of crystal. The rather open block structures were particularly suitable for these tactics.

If the lattice-imaging technique is to be extended to the study of crystals which have a less open and clearly projected structure, a rigorous theoretical basis for interpretation becomes indispensible. Lattice images at a sufficiently high degree of resolution to give some chance of displaying the positions of individual, highly scattering atoms (*ca.* 0.35 nm with current instruments, compared with the cation–cation distance 0.39 nm between apex-sharing octahedral groups) have hitherto been available only for the block structures. These have, accordingly, been the objects for calculations of image contrast as the electron optic theory has developed during the review period. The calculations have a much wider validity, however, for they define the conditions under which lattice images may be directly correlated with structure and thus now permit the technique to be employed for a wider range of chemically interesting systems. We therefore briefly discuss the relation between the recorded lattice image and the structure, seen in projection, of

[2] J. G. Allpress and J. V. Sanders, *J. Appl. Cryst.*, 1973, **6**, 165.

the observed crystal, before considering areas in which electron microscopy has shed new light on defect structures and chemical problems.

Theoretical Interpretation of Image Contrast.—In general terms, contrast in a micrograph reflects variations in the numbers of electrons falling upon the recording photographic emulsion; in an ideal optical system, the electrons arriving at a single point on the emulsion originate from a single point on the exit face of the object. The flux at each point on the emulsion depends upon the diffracting conditions within the crystal, upon instrumental factors, and upon operating factors. It is therefore possible to break down the theoretical problem of image formation from a large number of diffracted beams into three distinct parts: (*a*) calculation of the electron wavefunction at the exit face of the crystal; (*b*) modification of the wavefunction through the optical system, to take account of lens aberrations, moveable apertures, *etc.*; and (*c*) superimposed effects of operating adjustments and errors. Apart from the critical control of the orientation of the specimen, the major factor in (*c*) is the extent of under-focus; this is selected to compensate for the phase incoherence produced by spherical aberration and to give the best match between the observed image and that calculated theoretically.

Experimental experience has shown that useful lattice images are produced only from very thin crystals; even for crystals a few nanometres thick, realistic values for the intensity and phases of the various diffracted beams can be calculated only by using dynamical diffraction theory.[3] When lattice fringe images are formed by the combination of more than one or two diffracted beams (for which the electron optic theory is well established), the dynamical formulation of Cowley and Moodie[4] provides the most useful starting point for calculations.

The essence of this treatment is to consider the crystal to be divided into a number of thin slices perpendicular to the incident beam direction. The phase and amplitude of the incident wave is then modified by each slice. This is further simplified by considering each slice as a phase grating formed by projecting the potential distribution within each slice on to an internal plane. Fresnel diffraction then takes place between each grating. The treatment becomes less rigorous with increasing slice thickness, but provided this is kept small, no appreciable errors are found.[5] Thus, each time the electron wave passes across a slice, it is multiplied by a transmission function which is dependent upon the potential distribution in the plane.

If the potential of the nth slice, of thickness Δz, is $\phi_n(x,y,z)$ then the projected potential, $\phi_n(x,y)$ is given by

$$\phi_n(x,y) = \int_z^{z+\Delta z} \phi_n(x,y,z)\,\mathrm{d}z \qquad (1)$$

[3] J. M. Cowley, 'Progress in Materials Science', ed. B. Chalmers and W. Hume-Rothery, Pergamon, Oxford, 1967, Vol. 13, p. 267.
[4] J. M. Cowley and A. F. Moodie, *Acta Cryst.*, 1957, **10**, 609.
[5] G. R. Grinton and J. M. Cowley, *Optik*, 1971, **34**, 221.

The transmission function for the slice, the phase grating, is then defined as

$$q(x,y) = \exp(i\sigma\phi_n) \tag{2}$$

and gives the phase change imposed upon the wave as it passes the grating. The term in σ is a function of the relativistic electron wavelength λ of velocity v and the accelerating potential W, given by

$$\sigma = \frac{\pi}{\lambda W} \frac{2}{1 + (1 + \beta^2)^{1/2}} \tag{3}$$

where β is the relativistic correction term, v/c. The phase change between the planes must also be considered. This can be represented as $\exp[ik(x^2 + y^2)/2\Delta z]$ for the fast electrons that are involved. Adding these phase changes, by use of the principle of superposition, allows the wavefunction of the $(n+1)$th slice to be written in terms of the nth slice: thus

$$\psi_{n+1} = \left\{\psi_n * \exp\left[\frac{ik(x^2 + y^2)}{2\Delta z}\right]\right\} \exp(i\sigma\phi_{n+1}) \tag{4}$$

where $*$ represents convolution. The final wavefunction emerging from the crystal is obtained from equation (4) and an analytical solution can be derived.[4] The form this takes, however, is rather unsuitable for numerical computation, and an iterative scheme based on the equation for ψ_{n+1} has been used.[5–9]

In order to do this, it is convenient to handle the Fourier transform of equation (4), which is

$$U_{n+1}(h,k) = [U_n(h,k) \,.\, P(h,k)] * Q_{n+1}(h,k) \tag{5}$$

where $U_n(h,k)$ is the wave amplitude and phase from the nth slice, P is the propagation function

$$P(h,k) = \exp[2\pi i\zeta(h,k)\Delta z] \tag{6}$$

where $\zeta(h,k)$ is the excitation error, $(u^2 + v^2)\lambda/2$, for the (h,k) reflection in the reciprocal space co-ordinates (u,v), and $Q_{n+1}(h,k)$ is the Fourier transform of the phase grating function, $q_{n+1}(x,y)$ given by

$$Q(h,k) = \int_0^a \int_0^b q(x,y) \exp\left[2\pi i\left(h\frac{x}{a} + k\frac{y}{b}\right)\right] \mathrm{d}x\, \mathrm{d}y \tag{7}$$

The equation in U, equation (5), is evaluated for a sufficient number of slices to give the correct crystal thickness, and a sufficient number of beams so that the sum of the intensities is close to the incident-wave intensity. In the calculations referred to,[6–9] 435 beams were used in two-dimensional

[6] J. G. Allpress, E. A. Hewat, A. F. Moodie, and J. V. Sanders, *Acta Cryst.*, 1972, **A28**, 528.
[7] D. F. Lynch and M. A. O'Keefe, *Acta Cryst.*, 1972, **A28**, 536.
[8] G. R. Anstis, D. F. Lynch, A. F. Moodie, and M. A. O'Keefe, *Acta Cryst.*, 1973, **A29**, 138.
[9] M. A. O'Keefe, *Acta Cryst.*, 1973, **A29**, 389.

calculations. Normalization was 0.72 for a crystal thickness of 60 nm. This would be improved by including more beams, but at the expense of much greater computation time. The final result is to generate the diffraction pattern, which, because of the variable nature of Δz, is obtained as a function of thickness.

The contrast in the image is readily derived from the function U_n by another Fourier transform. If ψ_H is the Fourier transform of U_H so that

$$\psi_H(x,y) = F^{-1}U_H(h,k) \tag{8}$$

the image intensity is given by

$$I(x,y) = \psi(x,y).\psi*(x,y) \tag{9}$$

where F^{-1} is the inverse Fourier transform of $U_H(h,k)$, the amplitude and phase of the (h,k)th diffracted beam emerging from the crystal of thickness H. The representation of this image can be expressed in a variety of ways. The most immediately informative, however, is to plot out the expected contrast, using the half-tone print-out process developed by Head,[10] to give a computed micrograph.

These results relate to a perfect, aberration-free electron microscope, and they now have to be modified to take into account the instrumental and operational defects mentioned earlier. These are principally the inclusion of terms to account for the objective aperture, the spherical aberration of the objective lens, and the defect of focus employed. The objective aperture is represented by merely excluding all beams intercepted by the objective aperture from the final Fourier transformation. The spherical aberration acts so as to retard the phase of a beam passing through the lens at an angle α to the optical axis by an amount $\pi C_s\alpha^4/2\lambda$ with respect to the axial beam at the Gaussian image plane. C_s is the spherical aberration coefficient of the objective lens, which lies between 3 and 5 mm for most modern instruments. The defect of focus ε is taken into account by including a propagating function which is convoluted with the wavefunction at the exit surface of the crystal to allow the wavefunction at a distance ε from the exit surface to be obtained. Thus equation (8) becomes modified to

$$\psi_{H,\varepsilon}(x,y) = F^{-1}\{U_H(h,k).P_\varepsilon(h,k)\} \tag{10}$$

where P is a propagating function which accounts for defect of focus and spherical aberration, and is given by

$$P_\varepsilon(h,k) = \exp\{2\pi i\zeta(h,k)[\varepsilon - \lambda C_s\zeta(h,k)]\} \tag{11}$$

for a defect of focus ε and spherical aberration coefficient C_s. $\zeta(h,k)$ is the

[10] A. K. Head, *Austral. J. Phys.*, 1967, **20**, 557.

excitation error for the (h,k)th beam. Hence we can write the image wavefunction for an apertured system

$$\psi_{H,\varepsilon,n,C_s}(x,y) = \sum_h \sum_k U_H(h,k) \cdot \exp\left[2\pi i\left\{\zeta(h,k)[\varepsilon - \lambda C_s \zeta(h,k)] - \left(\frac{hx}{a} + \frac{ky}{b}\right)\right\}\right] \tag{12}$$

where the summations are carried out over the n beams supposed to pass through the aperture.

Other electron-microscope defects—chromatic aberration, the divergence of the incident beam, and astigmatism—can all be taken into account. However, these are found to be rather less important, and astigmatism in particular can be ignored for a carefully corrected modern objective lens. Equation (12) can then be used to compute an aberrated apertured image which in turn can be compared with the ideal one and with experimental results.

Calculations were first carried out for the case where only one row of diffracted beams, typically ($h00$ or $00l$), is excited.[5] These give one-dimensional information, and a set of parallel fringes results, which can be compared with experimental lattice images obtained under conditions which are matched by the data used in the computations. Some of the results of these calculations are compared with the experimental results in Figure 1.

There are no theoretical problems associated with computing two-dimensional images using the same procedure.[8] Once again, half-tone images are the easiest way of comparing the results of computations with experimental micrographs. Some examples are shown in Figure 2.

From these results it is possible to see that under certain circumstances the lattice images do represent accurately the structure of the crystal or, to be more precise, the projected charge density of the crystal. However, the calculations show that such an interpretation is not generally valid. In fact one must place severe limitations on the experimental technique used in order to avoid misinterpretation of lattice images. The most important limitation is that the crystal must be very thin, of the order of 10 nm. Of course, if the crystal thickness is accurately known, computations of contrast can still be made, but the image contrast does not reflect the crystal structure in simple terms and cannot be interpreted naively. Another very important result is that the most important microscope aberration appears to be spherical aberration, which causes severe perturbations of image contrast and necessitates rather careful selection of the objective aperture used. This is allowed for by computing images which are produced by beams having considerable phase retardation due to spherical aberration. This emphasizes, however, that lattice images can be interpreted intuitively only when care has been taken in obtaining the micrographs. The final criterion which must be carefully controlled is the defect of focus. For the lattice image to represent

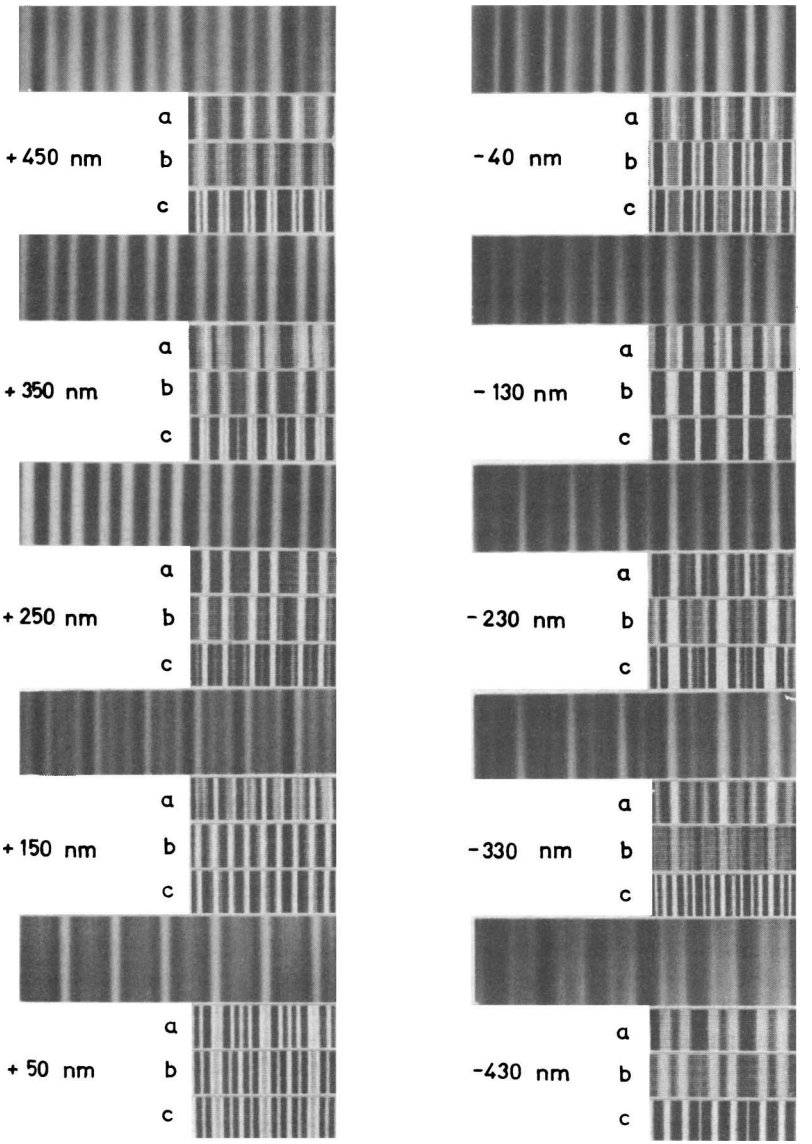

Figure 1 *Comparison of an observed through-focus series (larger images) and computed images (smaller), showing the effect of various instrumental factors. The numbers refer to the defects of focus for which the images were computed:* (a) *corrected for divergence and spherical aberration;* (b) *corrected for divergence only;* (c) '*ideal*' *image, with no corrections.*
(Reproduced by permission from *Acta Cryst.*, 1972, **A28**, 528)

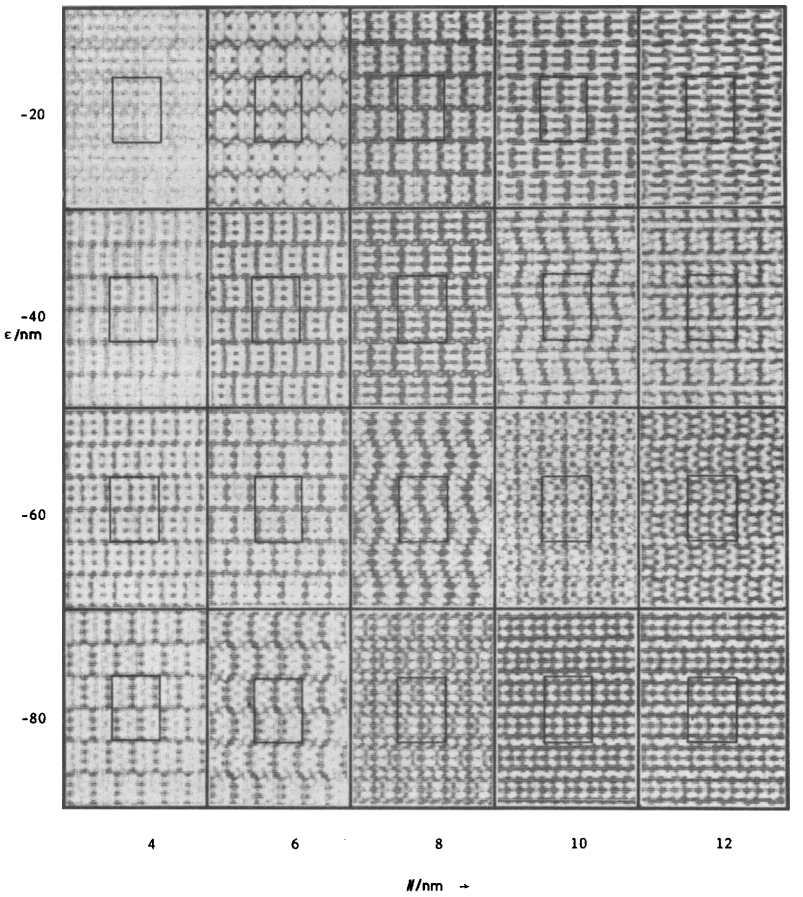

Figure 2 $Ti_2Nb_{10}O_{29}$ *n-beam lattice images showing the variation of contrast with crystal thickness,* H/nm, *and defect of focus* ε/nm. *The objective-lens spherical aberration coefficient,* $C_s = 1.5$ mm.
(Reproduced by permission from *Acta Cryst.*, 1973, **A29**, 389)

the crystal structure accurately, the microscope must typically be underfocused by about 80 nm. A degree of overfocus inverts the image contrast, but between these two positions, and outside them, the contrast varies in a rather complex way. Experimentally this is fairly easy to control, as the disappearance of Fresnel fringes at the edge of the crystal can be used to judge focus, and the correct defect of focus set by adjusting the objective lens by the appropriate amount. This is not necessary if the approximate crystal structure is known, for in that case the 'best' contrast can be judged by eye.

Such a procedure has been successfully used in the block structures, for example.

These results clearly show that it is highly desirable to compute images wherever possible. One problem of doing this is that the multislice computations are rather time-consuming. Some effort has thus been put into approximate computations which may be used to check the validity of structural models.[7]

The most useful of these approximations is the Projected Charge-density approximation, not only because of the relative simplicity of the calculations but also because of the attractive feature that image contrast can be related to charge density in the crystal on an intuitive basis. The experimental results and calculations have shown this to be possible in ideal circumstances, and it is therefore informative to compare calculations based on the charge-density model with the more accurate ones already described.

The approximation is based upon the theory of Fourier images derived by Cowley and Moodie.[11] This theory indicates that the periodic components of a two-dimensional phase object will produce a series of images at specific positions on either side of the object. In the electron microscope, these images have a magnification of approximately unity, and are spaced far enough apart for the normal focused image of the object to be the only one readily observed. A thin crystal can be considered as a simple phase object for the purposes of this approximation. The importance of the theory is that the intensity distribution in the image planes close to those of the Fourier images is given by[12]

$$I(x,y) = 1 - \frac{\varepsilon\lambda\sigma}{2\pi}\nabla^2\phi(x,y) \tag{13}$$

where I is the image contrast at defect of focus ε, $\phi(x,y)$ is the projected potential of the crystal, and λ and σ have been defined earlier. This equation holds for an unrestricted aperture and an idealized electron microscope. The potential distribution $\phi(x,y)$ is, however, closely related to the charge distribution in the crystal by Poisson's equation

$$\nabla^2\phi_p(x,y) \propto \rho_p(x,y) \tag{14}$$

Thus the image contrast for small values of ε can be written as

$$I(x,y) = 1 - k\varepsilon\rho_p(x,y) \tag{15}$$

where k is a constant. Hence the image contrast is a direct representation of the projected charge density in the crystal.

This equation is applicable to both periodic and non-periodic defects, and can be derived directly from equation (8)[6] by taking the high-voltage limit of the scattering. In this case, the wavelength tends to zero and the Ewald sphere becomes planar. The images should reverse their contrast on passing

[11] J. M. Cowley and A. F. Moodie, *Proc. Phys. Soc.*, 1958, **71**, 533.
[12] J. M. Cowley and A. F. Moodie, *Proc. Phys. Soc.*, 1960, **76**, 378.

through the Gaussian focus. However, the spherical aberration of the objective lens perturbs the contrast and it is found that underfocused images correspond rather better with the charge-density distribution. This is, of course, in agreement with experimental observations. Figure 3 shows a

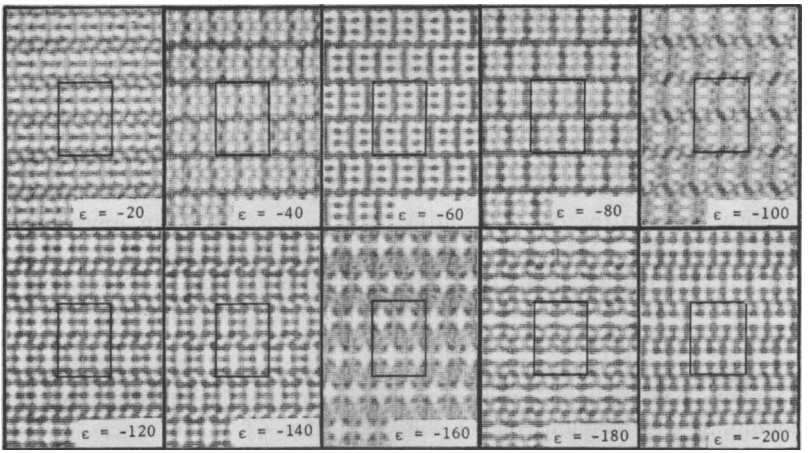

Figure 3 $Ti_2Nb_{10}O_{29}$ *n-beam lattice images for a crystal* 5 nm *thick at various values of defocus* ε/nm. *The objective-lens spherical aberration coefficient,* C_s = 1.8 mm
(Reproduced by permission from *Acta Cryst.*, 1973, **A29**, 389)

series of lattice images computed from the charge-density approximation for various values of defocus. It is possible to conclude, from such results, that for very thin crystals, provided that the image contrast reverses on passing through focus, the charge-density interpretation is valid. In this case, then, image features can be naively interpreted in terms of structural features that produce a variation in charge density. The thickness at which this approximation fails will depend upon the structure under consideration and the electron-microscope operating voltage; higher voltages are desirable in that the experimental conditions then resemble the conditions employed in the approximation more closely.

Experimental Observations of Lattice Images.—The theoretical calculations indicate that for very thin crystals the image contrast should be a representation of the charge density in the flake. Thus at medium resolution (*ca.* 1 nm) CS planes should appear darker than the background whereas at higher resolutions they should appear broken into segments representing the groups of edge-shared octahedra in the CS plane. This will be so regardless of whether the material is ordered or disordered, and the main advantage over *X*-ray crystallography lies in the consequence that the local order, instead of only an averaged order, can be observed. Electron microscopy is therefore

uniquely suited for the examination of such disordered materials, and for the detection of disorder that may not be apparent in *X*-ray diffraction.

A number of examples of the use of lattice fringe imaging were contained in the first Report in this series.[1] Since then a number of papers have been published which contain information obtained largely from this technique alone. Allpress,[13] in a study of WO_3 which had been doped with up to 10 mole percent Nb_2O_5, has observed disordered CS planes and numerous structural complexities in material which had proved to be difficult to study from the point of view of *X*-ray diffraction.

The results may be summarized in the following way. If the amount of Nb_2O_5 doped into WO_3 is fairly low, for example Nb_2O_5,38WO_3, the structure consists of fairly well ordered (210) CS planes. The bulk material is fairly close to the composition $(W,Nb)O_{2.975}$, and has an approximate formula $(W,Nb)_{40}O_{119}$. Increasing the niobium content causes the CS planes to change from (210) to (410) at compositions near to Nb_2O_5,18WO_3, that is $(W,Nb)O_{2.95}$ or $(W,Nb)_{60}O_{177}$, and ultimately to (100) when the niobium content is increased to Nb_2O_5,12WO_3. This has a composition near to $(W,Nb)_{14}O_{41}$, *i.e.* $(W,Nb)O_{2.929}$. In the intermediate compositions (510) CS planes have been observed. It is likely that careful control of annealing conditions and niobium content will yield other CS plane indices. Wavy CS planes have also been observed in these materials and are shown in Figure 4. These demonstrate in a striking fashion the power of lattice fringe imaging to reveal the underlying structure of disordered CS planes. The general pattern of these results has also been confirmed by Bursill and Hyde.[14]

It is interesting to note that at very low niobium contents, up to *ca.* 1 mol % Nb_2O_5, no CS planes are observed. It would seem likely that the Nb^{5+} ions will prefer an octahedral environment in the WO_3 lattice. Such a defect can be created by the insertion of an Nb^{5+} and an oxygen atom into the structure and this has been suggested by Gadó and Magnéli.[15] Such a defect can be considered as CS plane nucleus. If these link together, more extended CS plane segments will form. The real mechanism of formation of the CS phases is likely to be unrelated to this concept, but nevertheless the structural model is attractive as it avoids the necessity of introducing point defects into the system.

Rather less work has been done on the Ta_2O_5,WO_3 ternary oxides, although Bursill and Hyde[14] have done some preliminary electron-microscope studies. They found that CS phases are not so readily formed in this system as in the niobium–tungsten oxides, and only (310) CS planes were found.

The reason for these changes may possibly be associated with the different tendencies of W,Nb, or Ta atoms to form metal–metal bonds across shared octahedron edges. Blasse[16] has suggested a similar reason to account for

[13] J. G. Allpress, *J. Solid State Chem.*, 1972, **4**, 173.
[14] L. A. Bursill and B. G. Hyde, *J. Solid State Chem.*, 1972, **4**, 430.
[15] P. Gadó and A. Magnéli, *Materials Res. Bull.*, 1966, **1**, 33
[16] G. Blasse, *J. Inorg. Nuclear Chem.*, 1964, **26**, 1191.

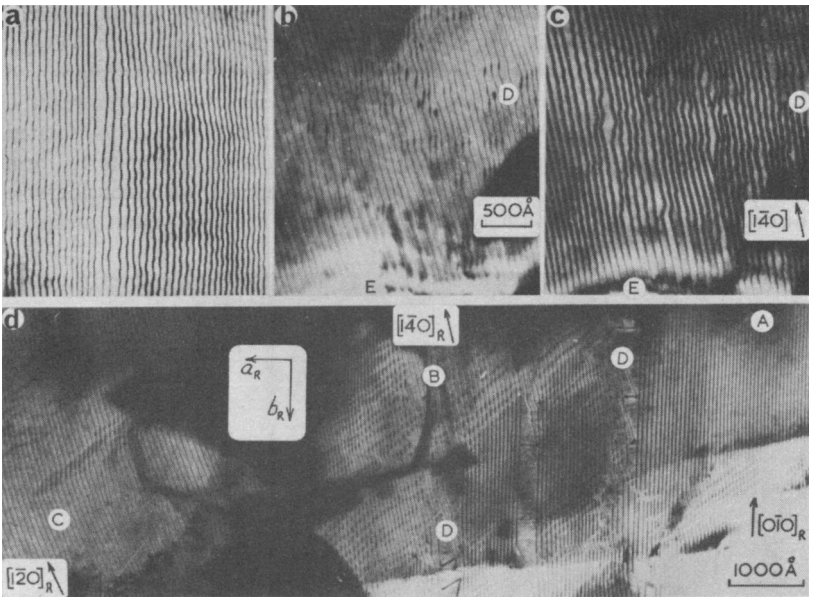

Figure 4 *Electron micrographs of fragments of crystals with a nominal composition* $Nb_2O : 11WO_3$. *The indices and directions refer to the* ReO_3*-type subcell which has the same orientation in all micrographs*
(Reproduced by permission from *J. Solid State Chem.*, 1972, **4**, 173)

structural differences between other mixed-metal oxides containing these M^{5+} ions. Any such model implies, however, that the ions doped into WO_3, Nb^{5+} or Ta^{5+}, are not arranged at random, but are preferentially distributed in the CS plane itself. No careful studies have been carried out to determine to what extent this is true. Indeed, such experiments will be difficult in view of the disorder normally found in the CS phases, and the fact that the *X*-ray scattering factors of the ions involved are all rather similar. Allpress,[13] however, has suggested that this may be so in the Nb_2O_5,xWO_3 oxides, basing his statement upon a comparison of computed and observed $h00$ structure factors for Nb_2O_5,$12WO_3$. The neutron-scattering lengths of the atoms differ more widely and, within the block structures $Ti_2Nb_{10}O_{29}$ and $TiNb_2O_7$ neutron diffraction has revealed a segregation of the two cation types, with Ti^{4+} not being distributed at random (see Section 4).

The nature of the structures found in the binary WO_{3-x} oxides has also been determined largely by lattice-image studies. The first Report in this series[1] suggested that the earliest stages in the reduction of WO_3 appeared to be the formation of (102) CS planes. These were generally isolated from one another, taking the form of Wadsley defects. However, it was mentioned that a possible precursor of this was the formation of CS planes on (100). Bursill and Hyde[14] have confirmed that (102) CS planes are normally observed

in WO_{3-x} and the evidence indicated that the presence of (100) planar faults in earlier studies[17] is not associated merely with oxygen loss in WO_{3-x}.

Further reduction in the binary tungsten–oxygen system is accompanied by extensive CS plane formation. Large WO_3 crystals lose oxygen readily. At temperatures below 900 °C the bulk structure initially contains isolated (102) CS planes. As reduction proceeds these CS planes aggregate to form quasi-ordered arrays in the WO_3 matrix, sometimes with considerable disorder. Figure 5 shows a typical fragment. The homologous series of

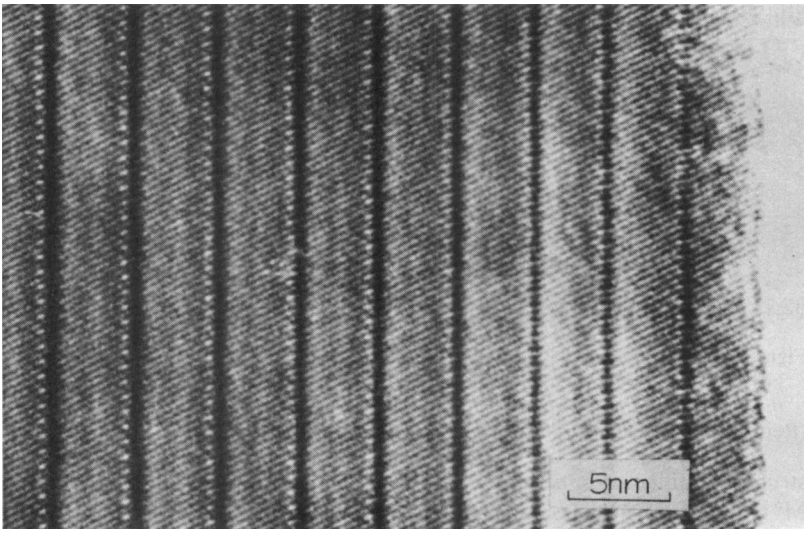

Figure 5 *Well ordered* (102) *CS planes* (*coarse fringes*) *in reduced tungsten trioxide. The crystal has been tilted a few degrees from a symmetrical* (*h*0*l*) *section to image the h*00 *planes* (*fine fringes*). *Note that the contrast in the CS plane changes as the crystal thickness increases*

oxides W_nO_{3n-1} is the ultimate result of this process. The range of n values seems to fall as low as ten or twelve, with a composition of approximately $WO_{2.90}$—$WO_{2.92}$. The (103) CS phases have not been observed to form within the bulk at these temperatures but appear as needles on the surface of the bulk crystals and at other places within reaction tubes. These most likely grow *via* a vapour-phase transport mechanism and are usually rather better ordered than the (102) CS planes. Figure 6 shows a well-ordered flake.

Bursill and Hyde[14] found fairly well isolated (103) CS planes in melted, slightly reduced samples of WO_3, suggesting that the structure type found

[17] J. Spyridelis, P. Delavignette, and S. Amelinckx, *Materials Res. Bull.*, 1967, **2**, 615; S. Amelinckx and J. Van Landuyt, in 'The Chemistry of Extended Defects in Non-metallic solids', ed. L. Eyring and M. O'Keefe, North-Holland, Amsterdam, 1970.

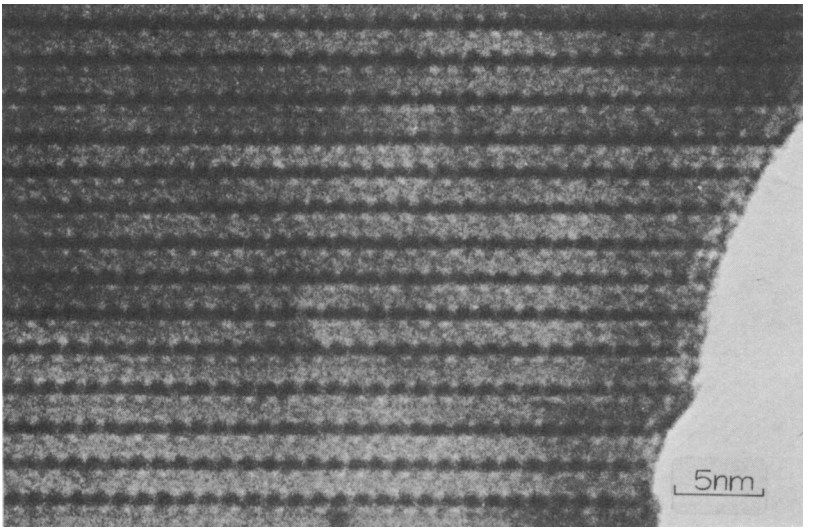

Figure 6 *Well ordered* (103) *CS planes in reduced tungsten trioxide. The composition of the flake is close to* $W_{18}O_{52}$. *The groups of six edge-sharing octahedra which constitute the CS plane are resolved as darker contrast*

may depend upon temperature. Recent experiments[18] have confirmed this speculation. Although sample preparation is more difficult at higher temperatures owing to the favoured formation of needle crystals from the vapour, selection of reduced fragments from large WO_3 crystals that have been carefully separated from needles shows that (103) CS planes can be found in the bulk. The conditions of formation depend upon both the temperature and the composition of the crystal. Sufficient data have not yet been accumulated to delineate this phase boundary carefully, but its position is clearly of great interest.

The oxides based upon the rutile structure have largely been understood by the use of electron microscopy. This is particularly so in the range of compositions close to MO_2 and in materials doped with altervalent cations. The study of Gibb and Anderson[19] on the $(Ga,Ti)O_{2-x}$ and $(Fe,Ti)O_{2-x}$ systems is typical of the power of CS plane imaging. In this work boundaries on (210) planes were found. In rather low concentrations of dopant, these were disordered, but in the Ga_2O_3,$x$$TiO_2$ oxides, fairly well ordered arrays of these planar faults were observed (Figure 7). These faults, when ordered, generate homologous series of compounds. In the case of the Ga_2O_3,TiO_2 oxides, these are of the formula $Ga_4Ti_{n-4}O_{2n-2}$. These faults are not CS planes in the normal sense, but do provide a mechanism for lowering the

[18] M. Sundberg and R. J. D. Tilley, *J. Solid State Chem.*, in the press.
[19] R. M. Gibb and J. S. Anderson, *J. Solid State Chem.*, 1972, **5**, 212.

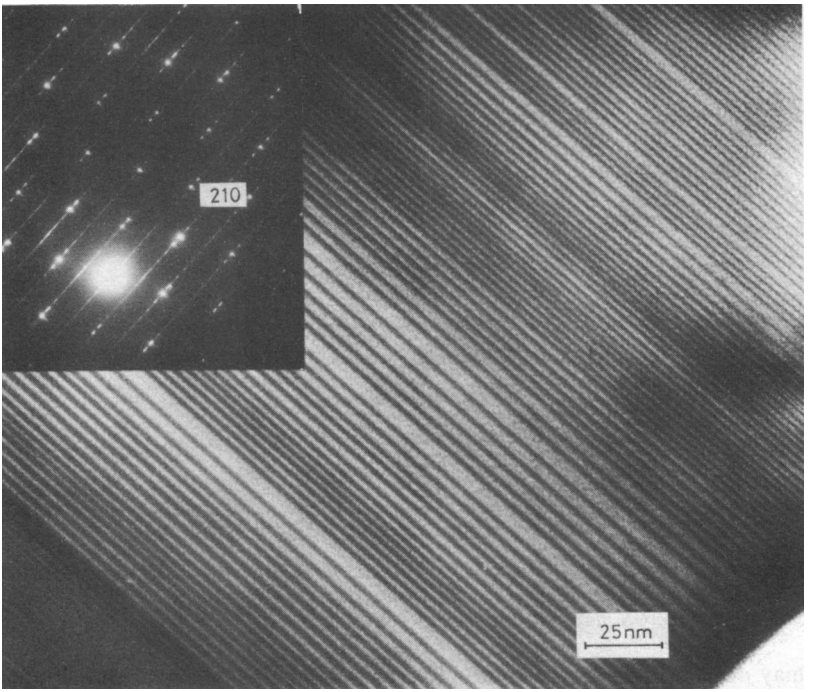

Figure 7 *Disordered faults on* (210) *planes in* TiO_2 *doped with* ca.12 atom % $GaO_{1.5}$ (Reproduced by permission from *J. Solid State Chem.*, 1972, **5**, 212)

anion to cation ratio in the material by a rather similar mechanism to the CS planes, that is, the introduction of extra 'interstitial' metal ions at the planar boundaries. This aspect of the CS phases is discussed in more detail in Section 3.

These results show that within the CS phases disorder and faulting is the rule rather than the exception. CS planes with variable spacing constitute coherent intergrowths of members of homologous series of compounds, and stoicheiometry is accounted for in this way rather than in terms of classical point defects. CS planes are also frequently found to end in the bulk. These terminate in a dislocation which provides a high-energy fault from which the CS plane can either grow or shrink. The terminating CS plane also provides another local region of stoicheiometric variability.

These features are also present in the block structures, which can be described (see Section 4) in terms of two nearly perpendicular sets of CS planes, which impose some constraints upon the flexibility of the system. Nevertheless, a very wide range of faulting has been found, often associated with the coherent intergrowth of two or more different block structures.

A number of recent papers show examples of such features in block

structures. Hutchison and Lincoln[20] have examples of linear defects and anomalous block sizes in crystals prepared by doping Nb_2O_5 with MgF_2. An example of these features is shown in Figure 8 together with an interpretation of the contrast.

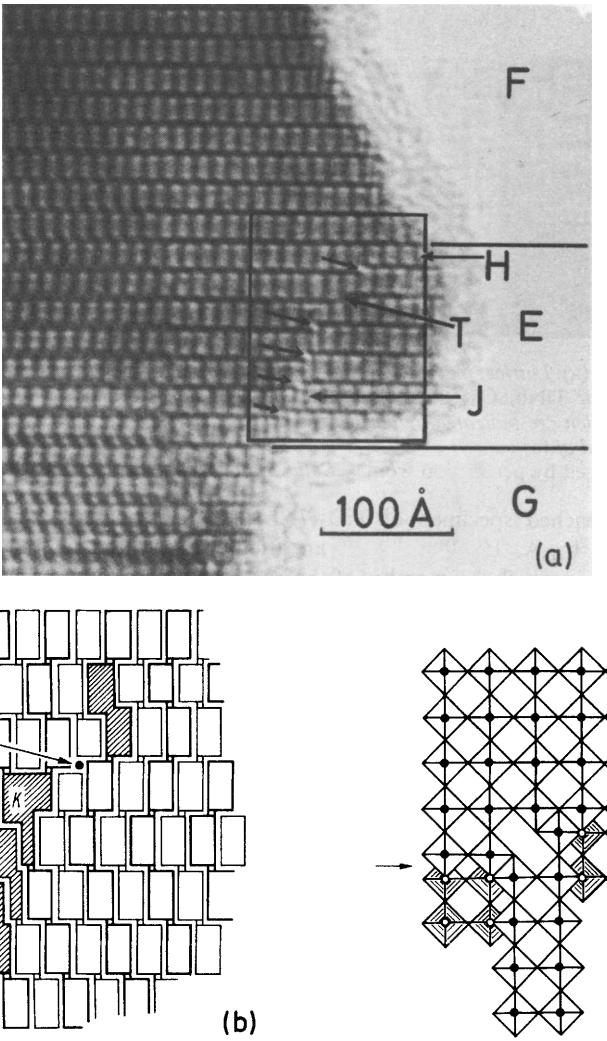

Figure 8 (a) *Lattice image of* $MgNb_{14}O_{35}F_2$ *showing* (001) *twinning and Wadsley defects*; (b) *Analysis of the structure within the enclosed area of* (a) *showing overlapping blocks and an anomalous block K*; (c) *Detailed structure of block K*
[Reproduced by permission from *Phys. Stat. Sol.* (*A*), 1973, **17**, 169]

[20] J. L. Hutchison and F. J. Lincoln, *Phys. Stat. Sol.* (*A*), 1973, **17**, 169.

In a remarkable series of papers, Iijima[21–25] has published high-resolution micrographs of mixed Ti–Nb oxides and H-Nb_2O_5 in which the component octahedra of the block structures are revealed. These provide conclusive proof that direct resolution of the structure of these materials is possible under the correct experimental conditions. Figure 9 shows an example from a study

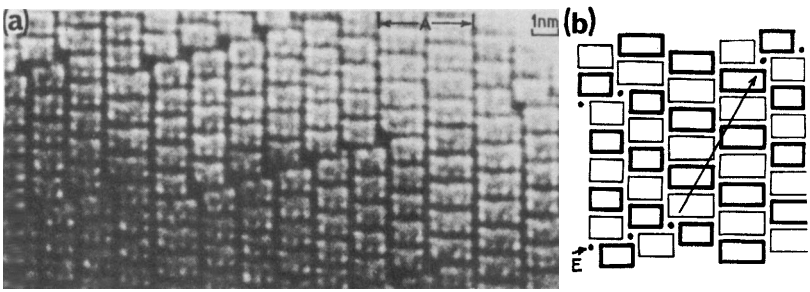

Figure 9 (a) *Lattice image showing the intergrowth of narrow domains of* 5×3 *blocks of* $TiNb_{14}O_{37}$ *and the displacement of planes* (E) *containing tetrahedral sites which are indicated by dark blobs of contrast*; (b) *Model of the region at the right end of* (a)
(Reproduced by permission from *J. Solid State Chem.*, 1973, **7**, 94)

of a quenched specimen of TiO_2,$7Nb_2O_5$. This material was originally prepared by A. D. Wadsley in an attempt to synthesize the compound $TiNb_{14}O_{37}$, which is a member of the homologous series of oxides $M_{3n}O_{8n-3}$ in which $n=5$. Although this compound was not identified in the original X-ray study, domains of the $TiNb_{14}O_{37}$ structure predicted by Wadsley have been found. The further implications of these studies are considered in Section 4.

The high-resolution micrographs illustrated in Figures 4–9 suggest that besides indicating the nature of faulting and intergrowths in these materials, direct structure determinations are possible. This is indeed so, and three studies can be chosen as illustrative of this extension of the technique.

Allpress *et al.*[24] have used direct lattice imaging to determine the structure of β-ZrO_2,$12Nb_2O_5$, another block structure. This present study is an extension, at higher resolution, of the earlier one of Allpress and Roth.[26] A lattice image is shown in Figure 10. From this it is a simple matter to derive an idealized structure to use as the basis for an X-ray study. The initial X-ray results confirm the postulated structure, and have allowed

[21] S. Iijima, *J. Appl. Phys.*, 1971, **42**, 5891.
[22] J. M. Cowley and S. Iijima, *Z. Naturforsch.*, 1972, **27a**, 445.
[23] S. Iijima, *Acta Cryst.*, 1973, **A29**, 18.
[24] J. G. Allpress, S. Iijima, R. S. Roth, and N. C. Stephenson, *J. Solid State Chem.*, 1973, **7**, 89.
[25] S. Iijima and J. G. Allpress, *J. Solid State Chem.*, 1973, **7**, 94.
[26] J. G. Allpress and R. S. Roth, *J. Solid State Chem.*, 1970, **2**, 366.

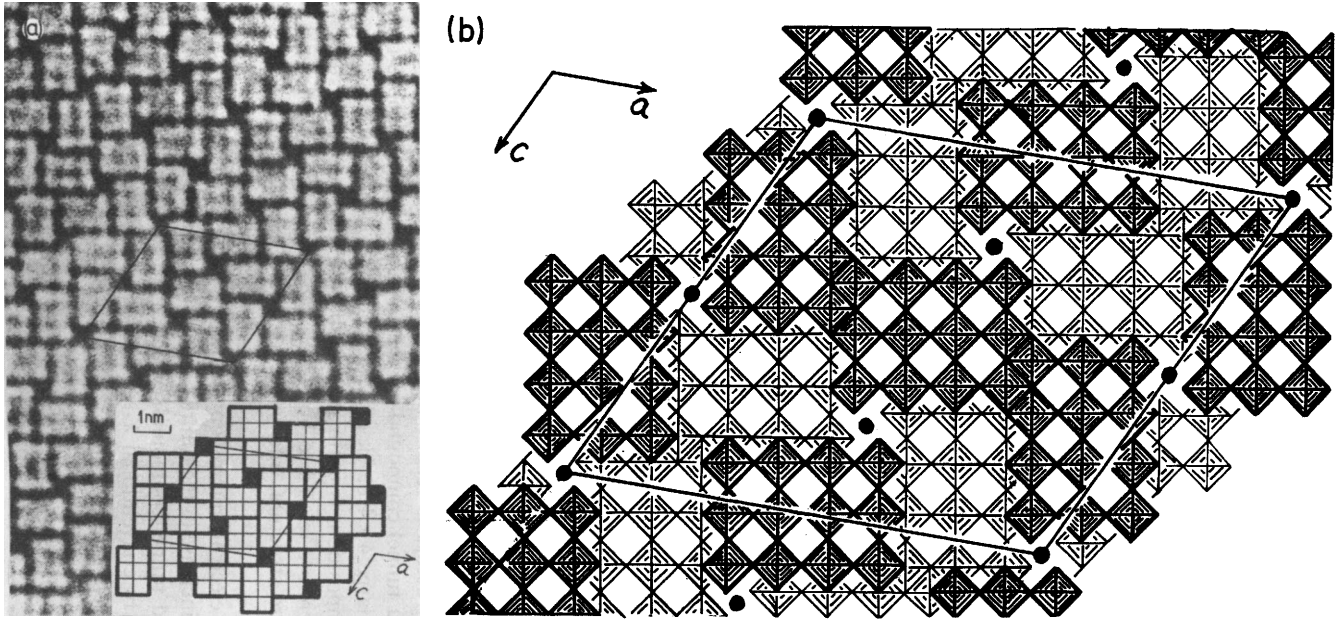

Figure 10 (a) *Lattice image from a thin fragment of* ZrO_2,$12Nb_2O_5$ *viewed down the b axis. The inset shows a schematic representation of the contrast.* (b) *Idealized model of the structure, derived from* (a)
(Reproduced by permission from *J. Solid State Chem.*, 1973, **7**, 89)

idealized structures of other polymorphs, particularly the γ-form, to be postulated.

In another study by Iijima[27] crystals with the more complex tungsten-bronze tunnel structure were examined. These structures are commonly formed in the Nb_2O_5,WO_3 system when approximately equal amounts of Nb_2O_5 and WO_3 react together. Figure 11 shows such a structure. This is a

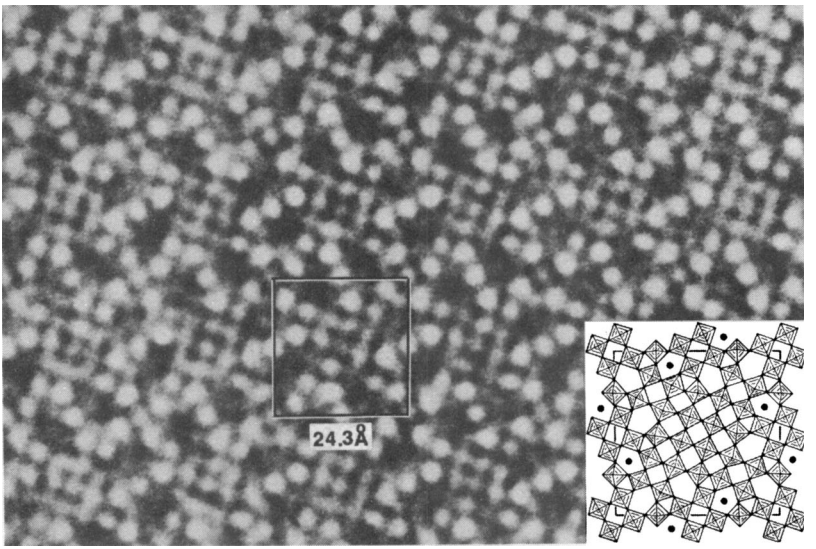

Figure 11 *Lattice image from a crystal of composition* $2Nb_2O_5,7WO_3$. *The inset shows the structure of this material, derived from the image contrast*
(Reproduced by permission from the 30th Annual Proceedings of the Electron Microscopy Society of America)

new structure, not yet determined by *X*-ray crystallography. Nevertheless, an idealized structure is readily derived from the electron micrograph. It is seen to be a tunnel compound related to the tetragonal bronze type but with a rather large 4×4 block of MO_6 octahedra at the centre of the unit cell. Its composition is estimated to correspond to $Nb_4W_7O_{31}$. The material is therefore related to both the block structures and the tetragonal tungsten-bronze structure, and is seen to be rather similar to the binary oxide $W_{18}O_{49}$.

The use of electron microscopy to derive idealized models of structures will probably increase in the future. This is likely to be so particularly in the CS phases and tunnel compounds which have large unit cells and are not easily handled by conventional *X*-ray techniques. The provision of a reliable idealized model reduces the complexity of the *X*-ray investigation

[27] S. Iijima, 30th Annual Proceedings of the Electron Microscopy Society of America, ed. C. J. Arceneaux, Los Angeles, 1972.

considerably. The technique is also of value for identifying small domains of phases which are not readily prepared in the form of homogeneous crystals large enough for *X*-ray determination. Further examples of this use of lattice imaging will be found in other sections of this Report.

Electron Microscopy and Lattice Imaging in the Study of Reactions.—The detailed observations in the preceding section can also be used as a basis from which to derive possible reaction mechanisms for the formation of CS phases. In the past this has usually taken the form of deducing the mode of CS formation in the parent oxides by an analysis of the configuration of CS planes in randomly selected crystal fragments. This approach was outlined in the previous Report.[1] A more recent paper, by Van Landuyt and Amelinckx,[28] is rather similar. From observations of thin films of TiO_2 they have suggested a mechanism of CS plane growth in which CS planes move into the foil as a pair, in a hairpin arrangement rather than separately. This mechanism may well hold in certain circumstances, but it seems unlikely that it is the only mechanism that will be applicable in the formation of CS phases. The variety of chemical compounds existing as CS phases and the widely differing atom mobilities found reinforce this concept. It therefore seems unlikely that one mechanism will be unique for all conditions of formation and all phases.

The model which appears to have the most general validity for the growth of CS planes into a bulk matrix is that described by Anderson and Hyde[29] although some minor modifications of this dislocation model have been suggested. It has been examined in greatest detail by Bursill and Hyde[30] who have considered the generation of CS planes in rutile. Using a ball model of the (100) plane of the rutile structure (idealized to give true hexagonal close packing of oxygen), they have 'grown in' CS planes by successive rearrangements of atoms. A sequence of time-lapse photographs taken with a cine camera allowed dynamic photographs of various possible reaction mechanisms to be obtained. In this way they have considered both the production of CS planes in rutile and the interconversion of various homologues one to another. These results have suggested a modification of the dislocation model in which an antiphase boundary is also involved in the movement of CS planes into rutile crystals. In this, the CS plane essentially nucleates at the surface and runs into the crystal along a path defined by an antiphase boundary.

These results do not rely to such an extent upon the high-resolution electron microscopy described in the previous sections. However, if such micrographs could be taken showing dynamical changes in the CS planes direct information upon mechanism could be found. A few such examples

[28] J. Van Landuyt and S. Amelinckx, *J. Solid State Chem.*, 1973, **6**, 222.
[29] J. S. Anderson and B. G. Hyde, *J. Phys. and Chem. Solids*, 1967, **28**. 1393.
[30] L. A. Bursill and B. G. Hyde, 'Progress in Solid State Chem.', ed, H. A. Reiss and J. O. McCaldin, Pergamon, Oxford, 1972, Vol. 7.

can be quoted here, in which changes take place naturally in the microscope under the combined influence of the electron beam and the surrounding vacuum of the electron-microscope column.

Iijima[31] has observed defects at this very high resolution while observing reduced crystals of $Nb_{22}O_{54}$. Figure 12 shows anomalous contrast at some block junctions. This contrast, which is attributed to tetrahedral atoms, gradually changes during observation. A model can readily be proposed from an examination of the micrographs, in which the tetrahedral Nb atoms are somewhat displaced to form perfect $Nb_{12}O_{29}$. Iijima has regarded this as a point-defect rearrangement, but in terms of lattice resolution it is possible that a chain of tetrahedral atoms exists in the matrix. The interpretation of lattice-image contrast would make this rather difficult to decide merely from inspection. If this latter supposition is correct, it then becomes quite closely related to the chains of atoms located between blocks which Anderson *et al.*[32] have characterized in the non-stoicheiometric compound $GeO_2{,}9Nb_2O_5$ (see Section 4).

The growth of (103) CS planes in a flake of a tungsten oxide of the W_nO_{3n-2} series under the action of the electron beam has been observed. The CS planes advance by extending along their length in accordance with the dislocation mechanism of Anderson and Hyde (Figure 13). However, a more complex rearrangement can also be seen where a loop of CS plane straightens somewhat and begins to grow parallel to the existing set. During the reaction two processes are seen to occur, the expansion of CS planes to the crystal edge, and some lateral movements to improve the ordering in the sample.

A final example of the use of electron microscopy as an adjunct to the study of reactions is provided by the studies of Anderson *et al.*[33,34] on the chemistry of niobium oxides. In a thermogravimetric study of the reduction of *H*-Nb_2O_5, the structural analysis was carried out by electron microscopy and diffraction, as *X*-ray techniques were not sufficiently sensitive to follow the behaviour. It was found that the course of the reaction, which traversed the composition range $NbO_{2.50}$—$NbO_{2.42}$, was structurally determined by the geometry of the starting phase. This was Nb_2O_5, with a block structure of (4 × 3) and (5 × 3) blocks. The first reaction to take place is one in which the (5 × 3) columns of ReO_3 structure in *H*-Nb_2O_5 are rearranged to (4 × 3) columns. At temperatures above 1100 °C the regions which contain only (4 × 3) blocks are able to intergrow with *H*-Nb_2O_5 to form the 1 : 1 intergrowth phase $Nb_{53}O_{132}$ before complete conversion into the more reduced material $Nb_{25}O_{62}$, which consists solely of (4 × 3) blocks. At lower temperatures the intergrowth is not formed, presumably because ordering the

[31] S. Iijima, 31st Annual Proceedings of the Electron Microscopy Society of America, ed. C. J. Arceneaux, New Orleans, 1973.

[32] J. S. Anderson, D. J. M. Bevan, J. M. Browne, A. K. Cheetham, R. Von Dreele, J. L. Hutchison, F. J. Lincoln, and J. Straehle, *Nature*, 1973, **243**, 81.

[33] J. S. Anderson and K. M. Nimmo, *J. C S Dalton*, 1972, 2328.

[34] J. M. Browne, J. L. Hutchison, and J. S. Anderson, 'Reactivity of Solids', 7th International Symposium on Reactivity of Solids, Chapman and Hall, London, 1972.

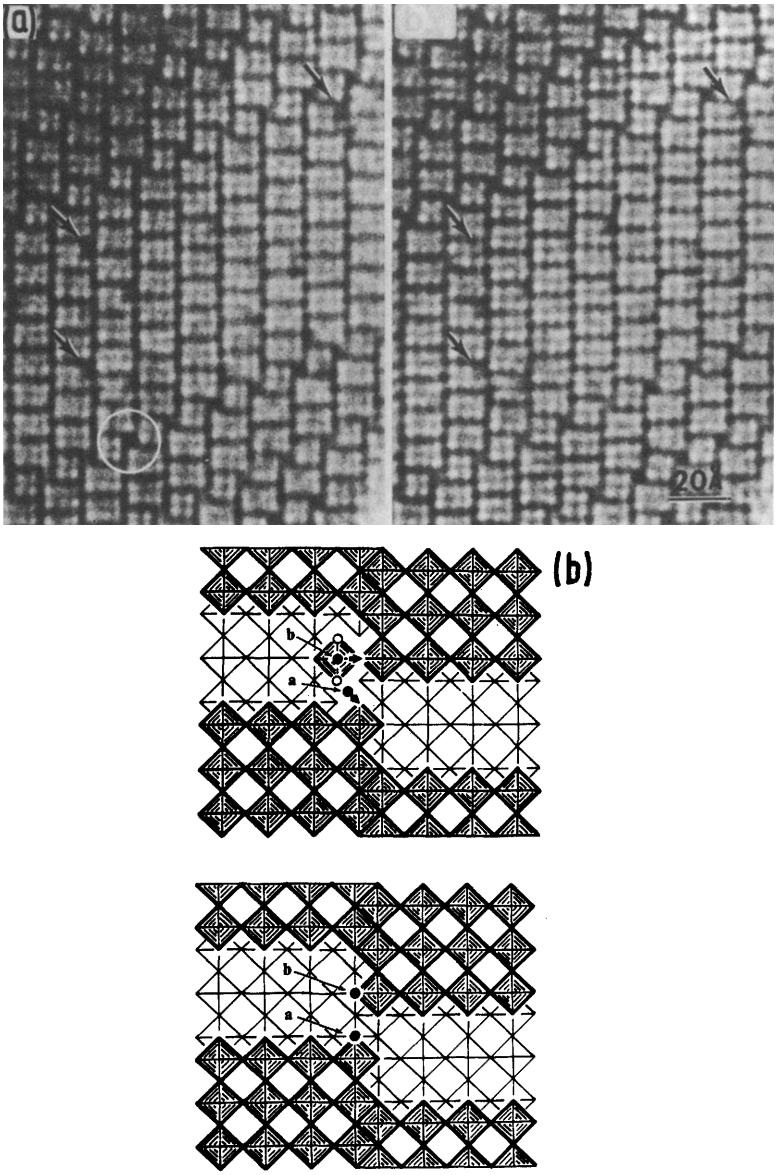

Figure 12 (a) *Successive lattice images showing defects which disappeared during observation.* (b) *A proposed model of the defect in* (a) *and its annihilation*
(Reproduced by permission from the 31st Annual Proceedings of the Electron Microscopy Society of America)

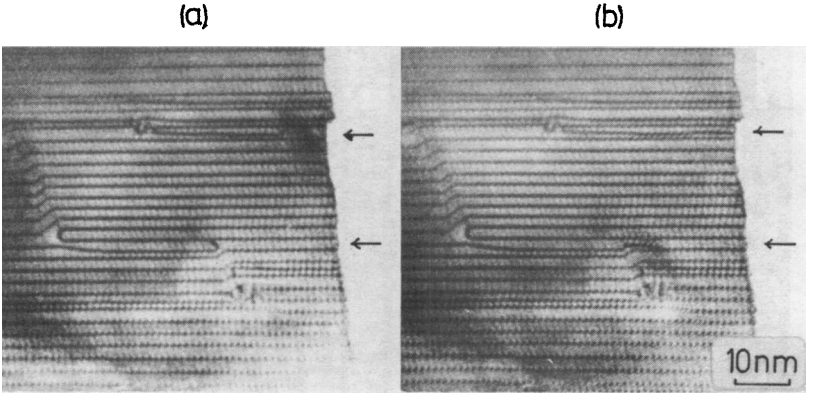

Figure 13 *Lattice images of* (103) *CS planes in reduced tungsten trioxide. The CS plane structure has altered during observation from that in* (a) *to* (b)

intergrowth has a higher activation energy. The process can then be written

$$\underset{(5\times3)_\infty+(4\times3)_1}{Nb_{28}O_{70}} \longrightarrow \underset{(4\times3)_2}{Nb_{25}O_{62}} \qquad \text{at 1000 °C}$$

$$Nb_{28}O_{70} \longrightarrow \underset{1:1\ \text{intergrowth}}{Nb_{53}O_{132}} \longrightarrow Nb_{25}O_{62} \qquad \text{at 1100 °C}$$

Further reduction proceeds by an analogous process, and can be formally written as

$$\underset{(4\times3)_2}{Nb_{25}O_{62}} \longrightarrow \underset{(4\times3)_\infty}{Nb_{12}O_{29}} \qquad \text{at 1000 °C}$$

$$\underset{(4\times3)_2}{Nb_{25}O_{62}} \longrightarrow \underset{1:1\ \text{intergrowth}}{Nb_{47}O_{116}} \longrightarrow \underset{(4\times3)_\infty+(3\times3)_1}{Nb_{22}O_{54}} \longrightarrow \underset{(4\times3)_\infty}{Nb_{12}O_{29}} \qquad \text{at 1100 °C}$$

The reaction takes place so as to preserve coherence in the block structures.

When the reverse process is considered, that is, the oxidation of $Nb_{12}O_{29}$ to Nb_2O_5, electron microscopy again is able to follow the reaction in a more satisfactory way than *X*-ray techniques. It was found that monoclinic $Nb_{12}O_{29}$ transformed to a new modification of Nb_2O_5, $Nb_{10}O_{25}$, with a (3×3) block structure, at the remarkably low temperature of 400 °C. The reaction proceeds *via* a superlattice phase which is a necessary part of the reorganization process. The lattice images reveal quite clearly the structure of the final Nb_2O_5 phase. It is apparent that this particular modification of Nb_2O_5 is produced because of the structural constraints of the parent phase, the low temperature of reaction making severe structural rearrangements unattractive. At higher temperatures it is conceivable that a different structural path will be followed, although this will not necessarily be the case.

3 Rotating CS Planes

CS Structures in the Titanium and Titanium–Chromium Oxides.—The earlier electron-microscope results indicated that CS planes displayed considerable disorder, with variable spacings between the CS planes. At this time it was believed that this variable spacing was the principal mode by which these materials accommodated variable composition. In the titanium oxides two series of compounds fell into this pattern. In the composition range $TiO_{1.75}$—$TiO_{1.90}$ a homologous series existed based on (121) CS planes, while between $TiO_{1.93}$ and TiO_2, (132) CS planes were found; these latter were ordered at the lower end of this range, but disordered near to TiO_2. The major problem to be solved was the structure of the region $TiO_{1.90}$—$TiO_{1.93}$, but it was believed that in this phase interval, $Ti_{10}O_{19}$, of the (121) series, coexisted with $Ti_{16}O_{31}$ of the (132) series. The spacings of the CS planes in these two phases are the same, although their orientation is different.

Bursill, Hyde, and Philp[35] have clarified the nature of this region and shown that change in stoicheiometry is accommodated in a far more subtle fashion. In the binary system electron-diffraction patterns suggested the existence of CS planes intermediate between (121) and (132), but these samples were heavily disordered and a study of the ternary system $(Ti,Cr)O_x$ was necessary to obtain a complete understanding of these intermediate CS phases.[35, 36]

It transpires that the CS plane orientation swings progressively from one orientation to the other in the phase range between the (121) and (132) ordered phases; this is more easily discernible in the ternary oxides than in the binary oxides. The structural geometry of these boundaries, which is considered in detail in the following section, shows how the CS planes in this intermediate range have indices (*hkl*) that can be resolved into segments of (121) CS plane alternating with segments of an antiphase boundary on (011). Each CS plane can thus be considered as an ordered intergrowth of units of (121) boundary and units of (011) boundary. The indices found vary from (132) through (253), (374), and (495) to (121). In the (253) series, most of the possible phases $(Cr,Ti)_nO_{2n-2}$ with n falling between 28 and 38 were observed, but other phases were identified, and in many cases departures from the (121) orientation can be so slight as to be discernible only by careful examination of diffraction patterns from crystals oriented to make the $[1\bar{1}1]$ zone clearly visible.

Attention may be drawn to some important features of these intermediate phases. The first of these is that the orientation (*hkl*) of the CS planes in any crystal is usually well defined, although the indices may be high. A change in composition can then be accommodated not only by a change of spacing between the CS planes, but also by a change in orientation, to produce a

[35] L. A. Bursill, B. G. Hyde, and D. K. Philp, *Phil. Mag.*, 1971, **23**, 1501.
[36] R. M. Gibb and J. S. Anderson, *J. Solid State Chem.*, 1972, **4**, 379.

new ordered phase. All the CS planes in this region have roughly the same spacing between CS planes: 1.61 nm between (132) CS planes in $Ti_{16}O_{31}$ and 1.60 nm for $Ti_{10}O_{19}$, of the (121) series. The spacing is more variable in the $(Ti,Cr)O_x$ oxides; for example, the (253) series covers a fairly wide composition range. In these phases, the spacing varies from 1.74 nm for $n = 28$ to 3.03 nm for $n = 48$.

There is also some uncertainty about the microstructure of these high-index CS planes. Bursill and Hyde have taken lattice fringe images of high-index CS planes which are clearly segmented into varying lengths of two components. For example, they have observed CS planes consisting of alternating segments of (132) and (253) orientation, whereas the diffraction pattern indicated a perfect CS phase based upon (385) CS planes. This clearly reveals both the averaging effect of the diffraction pattern and the power of lattice resolution. On some high-resolution photographs, though, the CS planes are straight. Thus the distribution of the unit segments making up these higher CS planes can be arranged either in regular sequence at the unit-cell level, or in a coarser distribution that can be likened more to a mixture.

In the binary system, the reversible behaviour found by Merritt for oxidation and reduction in the composition range $TiO_{1.9}$—$TiO_{1.93}$ and described in the earlier Report[1] can now be related to the structural changes described. Composition changes do not involve varying proportions of the two end members of the two CS series. Instead, a gradual reorientation of CS planes preserves good internal order without involving any change in the number of CS planes. This type of rearrangement is apparently structurally facile whereas the introduction or elimination of CS planes is a more difficult process which results in severe hysteresis in the partial molar free energy curve.

CS Structures in the Tungsten Oxides.—Far less work has been done on the tungsten oxides than on the titanium oxides. Experimental studies are outlined in Section 2, but it may be noted that the $(Nb,W)O_x$ system bears some analogies to the $(Ti,Cr)O_x$ system in that a continuous change of CS plane indices is found, from (103) to (001), over a relatively small change of composition. In the binary tungsten–oxygen system these changes are less easy to follow, and further studies are required before the system is as well understood as titanium oxides.

The Topology of CS Structures.—The results described above reveal a great variation in structural types amongst the CS phases already known. This complexity is more apparent than real and can be rationalized in terms of two lattice displacements, a lattice collapse and an antiphase displacement. The former is a pure CS operation and it alters the stoicheiometry of the crystal by a small amount. If, however, displacement lies parallel to the plane joining the two parts of the crystal, no change in stoicheiometry results but the cation rows in the two parts are mutually displaced. The complexity of CS plane types can now be constructed by intergrowing elements of

collapse and antiphase relation in varying proportions through the operation of the same displacement vector. It may be observed that the permitted displacement vectors must result in an identity operation when they act upon the anion sublattice. This is illustrated for the two principle systems of CS, the ReO_3 group and the rutile group.

ReO_3-related Structures. The structural geometry of the ReO_3 phases has been discussed by Bursill and Hyde.[14]

The ReO_3 lattice, shown in Figure 14, is able to collapse on one of the equivalent ($h00$), ($0k0$), or ($00l$) planes. A conservative displacement of the lattice can also occur without any change in stoicheiometry, the simplest being along one of the {101} set of planes. The commonly observed {102} and {103} CS planes can now be resolved into segments of both the ($h00$) and (101) boundaries. The indices of a CS plane ($h0l$) are given by the equation

$$(h0l) = p(001) + q(101) = (q, 0, p + q)$$

if the CS planes lie parallel to b and the 010 zone is considered. Hence

$$(102) = 1.(001) + 1.(101)$$
$$(103) = 2.(001) + 1.(101)$$

The amount of stoicheiometric change is governed solely by the amount of the component of collapse present, that is, the integer p, and the formula of a homologous series based upon a set of ordered (q, 0, $p + q$) CS planes is given by the formula M_nO_{3n-p}. The (102) and (103) series then are related to the series formulae M_nO_{3n-1} and M_nO_{3n-2}, as has been known since their discovery.

In the last two cases the value of p changes from 1 to 2, and the number of pairs of octahedra linked in each group, $p + 1$, changes from 2 to 3. This can be continued to give 4, 5, 6 ... pairs of linked octahedra. The resulting CS planes then lie on (104), (105), ($10p$) ... (001). These are illustrated in Figure 14.

This situation is found experimentally in the $(Nb,W)O_{3-x}$ oxides. For small niobium concentrations, the CS plane is {102} whereas for small tungsten concentrations the CS planes are on (001), although two intersecting sets are then always present and the oxides have block structures of the H-Nb_2O_5 type. At intermediate concentrations, the CS plane type changes progressively from {102} to {103} to {104} and so to one set of {001} CS planes when the niobium concentration is of the order of 10 mole per cent.[13]

Any CS plane lying between any adjacent pair of CS planes in the group above with $q = 1$ must embody some units of each of the adjacent pairs. Thus the plane of lowest index between (102) and (103) is (205), constructed by combining units of (102) and (103) structure alternately along the CS planes. Similarly the next lowest are (307) and (308), which are made up of two units of (102) plus one of (103) and two units of (103) plus one of (102) respectively as shown in Figure 15.

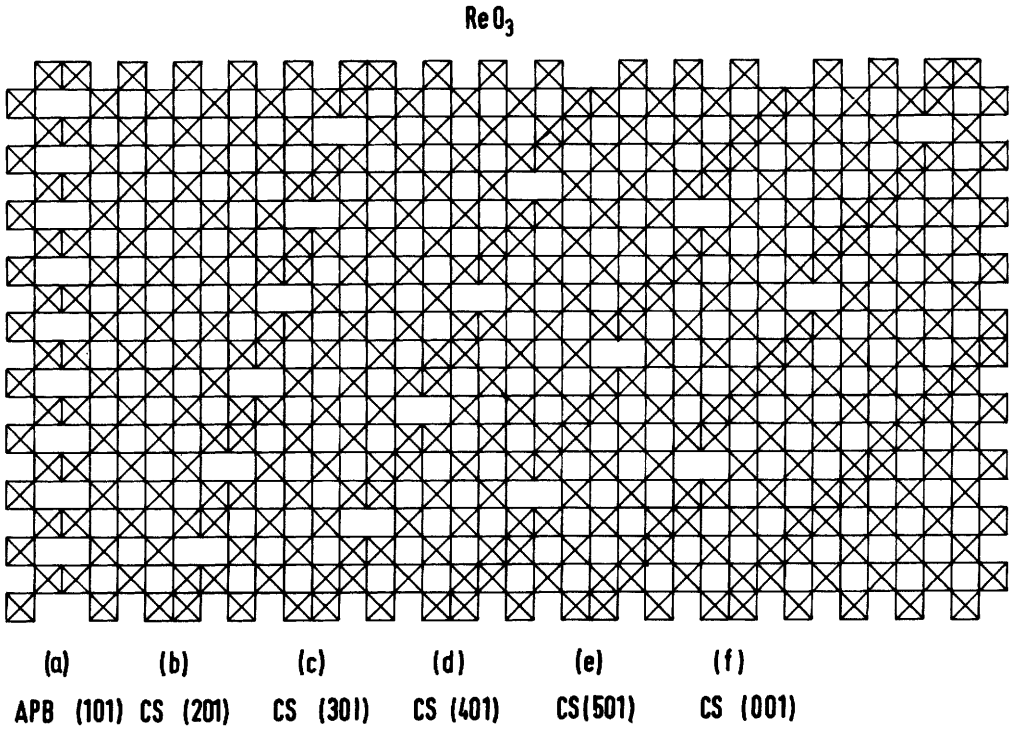

Figure 14 *Crystallographic shear in the* ReO_3 *structure.* (a) *Antiphase boundary on* (101); *crystallographic shear on* (b) (201), (c) (301), (d) (401), (e) (501), *and* (f) (001)

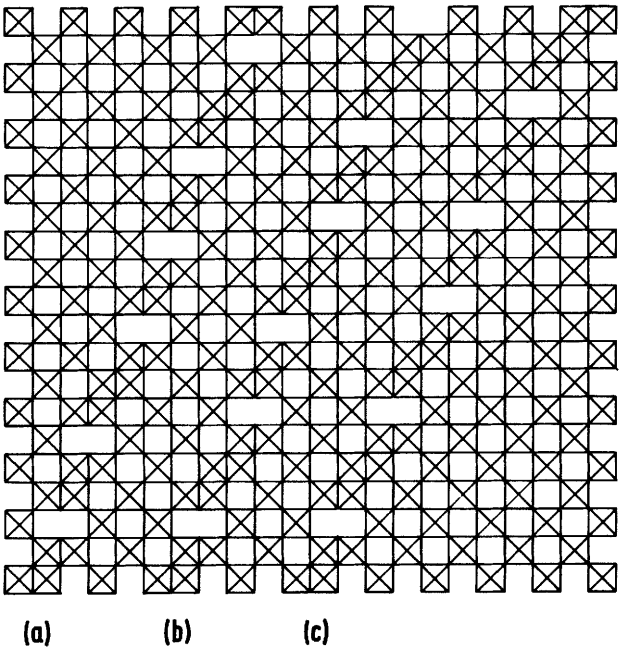

Figure 15 *Crystallographic shear in the* ReO_3 *structure on* (a) (703), (b) (502), *and* (c) (803)

In these cases with $q > 1$, the number of edge-shared pairs of octahedra in a unit of CS plane is $(p+q)$, and they are arranged in q separate groups. If the alternating groups are not ordered, the CS plane will either wander between the two end members or be resolved into zig-zag sections, depending upon the CS plane groupings.

As a result of these possibilities, almost any stoicheiometry could be accommodated within an ordered CS structure; it is also possible that a given stoicheiometry may be achieved in more than one way; thus the composition $WO_{2.91}$ can be made from either an ordered (102) or a (103) CS structure. This aspect of these phases will be considered again later.

Rutile-related Structures. The rutile structure can be regarded as derived from an MO_3 parent of the PdF_3 structure type, by the recurrent operation of a CS vector $\frac{1}{3}[112]/(100)_{PdF_3}$. If the collapse is upon the (001) planes, with a vector $\frac{1}{3}[121]$, the α-PbO_2 structure results.

Since the previous Report, Bursill and Hyde[30] have clarified the structural geometry of the rutile-based CS phases so as to remove much of the complexity of the experimental results. For this they idealize the oxygen packing in the rutile structure, from the puckered arrangement found in practice to perfect h.c.p., by flattening on $(h00)$ or $(0k0)$. If the $(h00)$ planes are flattened, they become the $(00l)$ planes of the hexagonal lattice and the CS vector $\frac{1}{2}[0\bar{1}1]$

in the rutile lattice remains a perfect oxygen–oxygen vector. A diagram of this idealized structure is shown in Figure 16.

The CS planes observed in the rutile system, either in the binary titanium oxides or in the ternary doped titanium oxides can be summarized as lying between (121) and (132), including both these extremes. As with the ReO_3 oxides discussed above, their orientation can be described in terms of two elementary operations: a CS operation and a stoicheiometric fault of the antiphase boundary type. An intergrowth of these produces the variations observed.

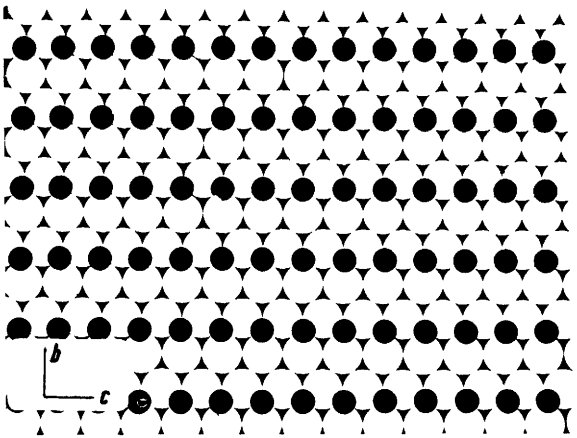

Figure 16 *A* (100) *layer of idealized rutile*

An antiphase boundary (APB) is produced by the vector $\frac{1}{2}[0\bar{1}1]$ operating on (011). The strings of edge-shared octahedra are stepped across the APB as can be seen from Figure 17. It is convenient to represent such a boundary of steps by the sequence

.....///////.....

The same fault vector, $\frac{1}{2}[0\bar{1}1]$, operating on (121) eliminates oxygen sites from the rutile structure. The structure of the (121) CS plane so formed differs from the APB described above in having an extra cation at each step along the trace of the boundary. This extra cation is not to be regarded as a point defect in any sense: it is an integral part of the structure. If one is to equate anything with a defect in the rutile lattice it should be the CS plane as a whole. Representing the CS step by the symbol ∇, which denotes the folding of the cation strings into a Z shape, the trace of the CS plane on (100) can now be represented as

.....∇∇∇∇∇.....

Ordered sequences of ∇ and / units can be formulated as has been done by Bursill and Hyde;[30] the number of possible ordered combinations of these

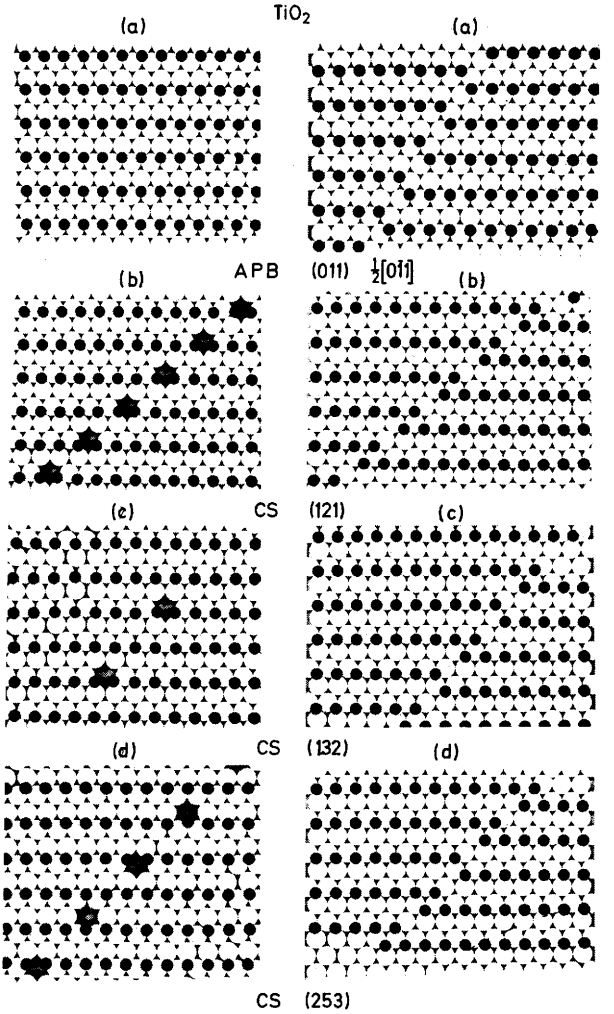

Figure 17 *Crystallographic shear in the rutile structure. The structures on the left show the pattern of vacant oxygen sites needed for subsequent collapse to produce the structures on the right*: (a) *an antiphase boundary on* (011); *crystallographic shear on* (b) (121), (c) (132), *and* (d) (253). *The displacement vector for* (a) *to* (d) is ½[01̄1]

two elements is very large. Of special interest are the (121) and (132) CS planes found in the rutile system. The latter represents an ordered array of APB (/) and collapse (∇) components:

$$\ldots\ldots\ldots/\nabla/\nabla/\nabla/\nabla/\nabla/\ldots\ldots\ldots$$

The structures and the indices of the swinging CS planes lying between (121) and (132) and found in the $(Cr,Ti)O_{2-x}$ oxides are those obtained by

the intergrowth of different proportions of these (121) and APB components. Some of these possibilities are shown in Table 1; Figure 17 shows idealized (100) layers representing some of these structures. The composition of each series of oxides formed from a regular sequence of these CS planes depends upon the number of collapse units found in each CS plane. The formulae of some series of oxides formed are shown in Table 1.

Table 1 *Some possible structures formed by the ordered intergrowth of elements of antiphase boundaries and* (121) *CS planes in titanium oxides based on the rutile structure*

Sequence of structure elements along CS plane trace	*CS plane indices*	*Homologous series*
.../////////...	(011)	Ti_nO_{2n}
.../▽/▽/▽/▽/▽/...	(132)	Ti_nO_{2n-1}
.../▽▽/▽▽/▽▽/▽▽/...	(253)	Ti_nO_{2n-2}
.../▽▽▽/▽▽▽/▽▽▽/▽▽▽/...	(374)	Ti_nO_{2n-3}
.../▽▽▽▽/▽▽▽▽/▽▽▽▽/...	(495)	Ti_nO_{2n-4}
...▽▽▽▽▽▽▽...	(121)	Ti_nO_{2n-1}
...▽/▽/▽/▽/▽/...	(132)	Ti_nO_{2n-1}
...▽//▽//▽//▽//▽...	(143)	Ti_nO_{2n-1}
...▽///▽///▽///▽...	(154)	Ti_nO_{2n-1}
...▽////▽////▽////▽...	(165)	Ti_nO_{2n-1}
.../////////...	(011)	Ti_nO_{2n}

α-PbO_2-related Structures. In a consideration of the CS planes in rutile, units of the (011) antiphase boundary were intergrown with units of the (121) CS plane. If the (011) boundary is considered in isolation it causes a step in the cations parallel to the rutile *c* axis; By introducing such a boundary on every alternate (011) anion plane, the α-PbO_2 structure is generated (Figure 18). The α-PbO_2 structure has the same hexagonal close-packed array of oxygen atoms as in rutile, but with a staggered zig-zag arrangement of the strings of edge-shared cation–anion octahedra. It can be regarded as an ordered polysynthetic rutile. If the (011) boundaries are inserted on every anion plane, a twinned orientation of rutile is found.

In the first Report, CS operations in the α-PbO_2 structure were considered from a geometrical point of view. At that time, no CS phases based upon this structure had been reported. Since then Grey and Reid[37] have published a fairly detailed study of phase relations in the system Fe–Cr–Ti–O. For certain compositions both pseudobrookite phases and oxides based on (121) CS in rutile were recorded, but they found a series of structures with a general formula $(Cr,Fe)_2Ti_{n-2}O_{2n-1}$ over much of the phase range. These were

[37] I. E. Grey and A. F. Reid, *J. Solid State Chem.*, 1972, **4**, 186.

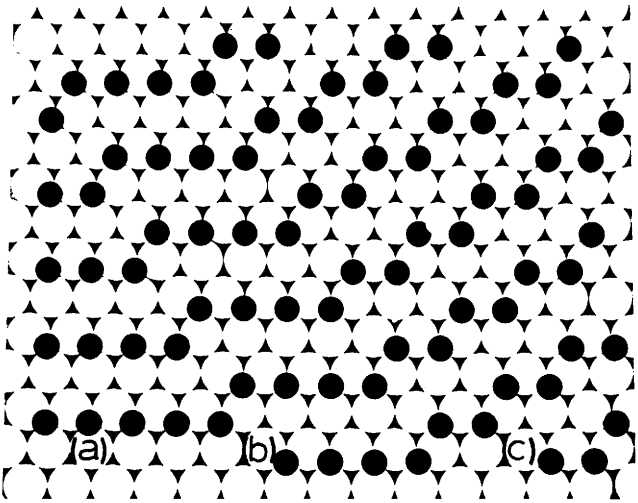

Figure 18 *A* (100) *layer of idealized rutile* (a), *containing* (b) *a single* (011) *antiphase boundary and converting into* (c) *a lamella of the* α-PbO_2 *structure*

members of a homologous series of oxides based upon CS in an α-PbO_2 parent.

The structures of these phases were established through consideration of the structure of V_3O_5,[38] which was found to be isostructural with$(Cr,Fe)_2TiO_5$, and a determination of the structure of the M_4O_7 homologue, $CrFeTi_2O_7$.[39] The V_3O_5 structure can, in fact, be regarded either as $n = 3$ in the (121) CS phases derived from rutile or as $n = 3$ in a series based upon (110) CS planes in an α-PbO_2 parent. The higher homologues $n = 4$ and 5 are also derived from the same model, with an increased spacing between the CS planes.

Besides these phases, ordered intergrowths have also been found between the M_4O_7 homologue and the members on either side, M_3O_5 and M_5O_9, and these can be written as series of oxides $(M_3O_5)_m(M_4O_7)_n$ and $(M_4O_7)_n(M_5O_9)_n$. Because of their similar structures all these intergrowth phases give very similar *X*-ray powder patterns. Grey and Reid have suggested that the apparent range of homogeneity shown by the ternary phase $Cr_2Ti_2O_7$ may well be explained on this basis. It would be very difficult, from powder *X*-ray work alone, to identify such intergrowth structures, even if they were perfectly ordered.

The α-PbO_2 structure is a high-pressure polymorph of rutile, and the CS planes in these homologues can be considered to stabilize this structure to atmospheric pressure. The width of the slabs which can be stabilized in this way is limited, and in these materials does not exceed that of the $n = 5$ oxide.

[38] S. Åsbrink, S. Friberg, A. Magnéli, and G. Andersson, *Acta Chem. Scand.*, 1959, **13**, 603.
[39] I. E. Grey and W. G. Mumme, *J. Solid State Chem.*, 1972, **5**, 168.

The somewhat larger zirconium ion can be made to replace titanium in these compounds to a limited extent, and such a substitution permits homologues with $n > 5$ to be made.

Rotary Crystallographic Shear.—The foregoing geometrical consideration of the CS phases as ordered intergrowths of simple end members is of more value than just a classification; it suggests both possible reaction mechanisms and relationships between the compounds which do not form CS phases and those that do. These in turn are then useful for predicting chemical behaviour.

One of the most elegant of these geometrical relationships has been described by Bursill and Hyde.[40] This relates the cubic ReO_3 structure to the complex tunnel structures of the tungsten bronze type. These are found in the tungsten–oxygen system, where WO_3, which has a slightly distorted ReO_3 structure, forms tunnel compounds on doping with an alkali metal. Similar structures exist in the complex tungsten–niobium and tungsten–tantalum oxides and in many other ternary niobium and tantalum oxides.

The relationship between the ReO_3 parent and the tetragonal tungsten bronze structure is shown in Figure 19. The basic operation required is the

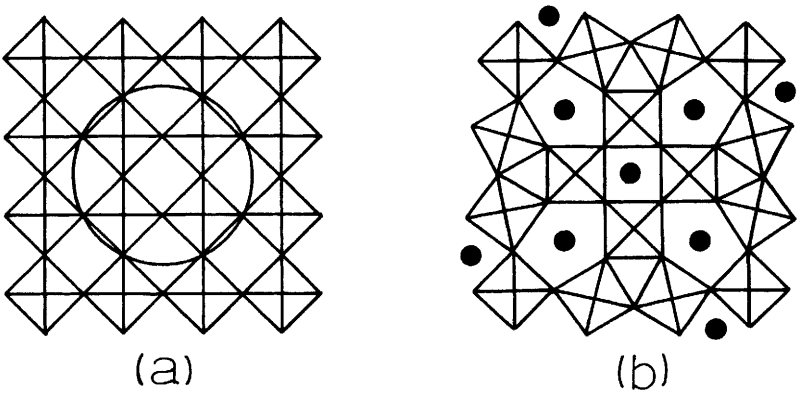

Figure 19 *The formation of the framework of the tetragonal tungsten bronze structure* (b) *from the* ReO_3 *structure* (a) *by rotation of the circled unit by* 45°, *interpolating alkali-metal atoms* (●) *in some tunnels*

rotation of a column of ReO_3 octahedra by 45°. In some ways this is akin to the generation of an antiphase boundary in ReO_3. In this case, however, the antiphase boundary has changed from a planar fault into a narrow cylinder, an antiphase column. This operation produces pentagonal tunnels. The relative positions of the rotation centres of the antiphase columns now yields a variety of groupings of pentagonal or, if a suitable juxtaposition is arranged, hexagonal tunnels, which can now form the frameworks both of the bronze structures already characterized and of a large number of hypothetical

[40] L. A. Bursill and B. G. Hyde, *Nature Phys. Sci.*, 1972, **240**, 122.

structures. The real structures differ from these idealized frameworks in that the metal–oxygen polyhedra are distorted, and the tunnels frequently contain additional cations. These are not introduced by the simple rotation, which preserves the MO_3 stoicheiometry of the parent, but may be important in stabilizing a more open skeletal structure.

There is a close relationship between the ReO_3-based CS phases and the tunnel structures. Both are formed by reduction of a hypothetical or real ReO_3 parent. The range of composition over which the CS phases are favoured depends on the material studied. For MO_{3-x} this is approximately MO_3—$MO_{2.88}$, and the CS structure formed depends upon the metal M present. The niobium oxide block structures have a range $MO_{2.70}$—$MO_{2.3}$. Both systems form tungsten bronze or related structures when these limits are exceeded (compositions MO_3—$MO_{2.5}$) and coexist with the rutile structure when the composition is below $MO_{2.3}$. The degree of reduction is not the only variable; large cations with a low charge, the alkali metals, and alkaline earth metals tend to force the ReO_3 matrix to adopt a tunnel structure over quite substantial composition ranges, whereas the smaller, more highly charged transition-metal ions are more tolerant of the CS phase structure. This may well be in part due to size effects, plus the fact that transition-metal ions in general have an energetic preference for octahedral co-ordination. The larger M^{1+} and M^{2+} ions cannot fit so readily into an almost close-packed oxygen array and force the structure type to change more drastically.

These variables are not the only ones to consider. The oxide $W_{18}O_{49}$ has a structure which can be best described as a tunnel structure, but which is derived from an ReO_3 parent by a combination of rotation and planar CS operation. The questionable valence of the tungsten cations in this structure makes it difficult to suggest that size or low valence themselves are responsible for these structural changes, and further experiments may well show more subtle causes.

As the composition of the transition-metal oxides approaches MO_2, the stable structure type becomes, in most cases, the rutile structure, into which rotation faults of the same type as in the ReO_3 matrix can be introduced. These form the basis for a series of compounds in many ways analogous to the tungsten bronzes, the hollandites, typified by the manganese oxides $A_xMn_8O_{16}$, where A can be a large uni- or bi-valent ion, Ba^{2+} being typical. The generation of these structures is shown in Figure 20.

There are close parallels between the formation of the hollandites and the tungsten bronzes. In both, cations of low valence and large radius, which cannot occupy octahedral interstices, are introduced into a fairly close-packed oxygen array. If the cations are smaller and more highly charged, they can fit in, and either form mixed rutiles or trirutiles or else develop CS phases based upon the TiO_{2-x} or α-PbO_{2-x} structure types. As before, simple considerations of size seem insufficient at this stage to account for all the observations and more subtle forces may be responsible.

The rutile structure type can also be related topologically to the fluorite

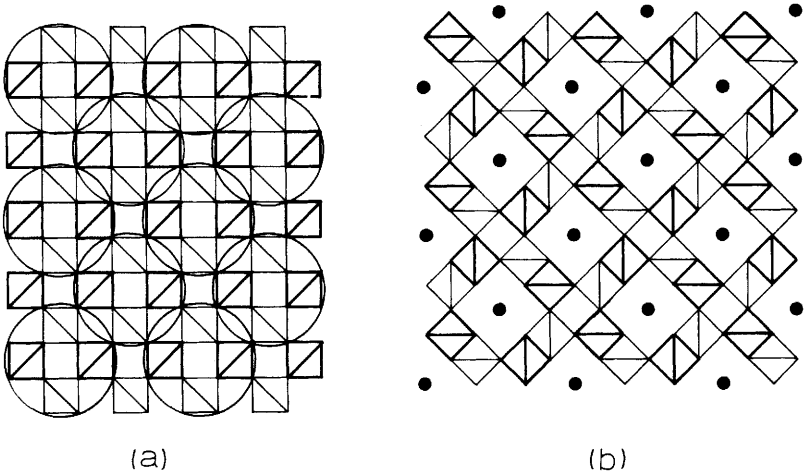

Figure 20 *The formation of the hollandite structure* (b) *from the rutile structure* (a) *by rotation of the units circled by* 45° *and interpolating metal atoms* (●) *in the tunnels. The* $[MO_6]$ *octahedra are idealized to squares in this projection*

structures.[41] CS has not been found hitherto in the fluorite-related phases, but has been discussed by Hyde[42] as being relevant to the chemistry and possible CS transformations of UO_2 and related phases.

4 Block Structures

The Topology of Block Structures.—It is possible to extend the foregoing discussion of the structure and rotation of crystallographic shear planes to give a rationale for the block structures found in the niobium oxides and related compounds. Their characteristic is that they are built up from rectangular columns of ReO_3 structure, measuring $m \times n$ octahedra in cross-section and infinite in length. The octahedrally co-ordinated cations are at different levels ($z = 0$ and $z = \frac{1}{2}$) in adjacent columns, so that they share octahedron edges at the interface between columns. These interfaces thus have the structure of a short segment of {100} CS plane. A perfectly ordered structure can be adjusted to subtle variations of composition by changes in the cross-section and linkage of the columns,[1] which change the number of anion sites eliminated by octahedron edge sharing.

This extensive set of elegant, but at first sight complex, structures can be related to the parent ReO_3 structure type by the simultaneous, recurrent operation of two nearly orthogonal CS operations: $(\frac{1}{2}a)[011]/(h0l)$ with $l > h$ and $(\frac{1}{2}a)[\bar{1}10]/(h'0l')$ with $h' > l'$. In defining these CS operations, the

[41] B. G. Hyde, L. A. Bursill, M. A. O'Keeffe, and S. Andersson, *Nature Phys. Sci.*, 1972, **237**, 35.
[42] B. G. Hyde, *Acta Cryst.*, 1971, **A27**, 617.

displacement vector and the crystallographic shear plane are stated, here and subsequently, in terms of the uncollapsed ReO_3 structure. Except for {101}, any oblique (*h*0*l*) plane intersecting the square (010) cation lattice of the ReO_3 structure necessarily has its trace divided into segments; for $l > h$, these consist of steps with treads parallel to (001) and risers, of unit height, parallel to (100). Writing $l/h = I + R/h$, where I is an integer and $0 \leqslant R < h$, the segments will consist of R steps of length $(I + 1)$ and $(h - R)$ steps of length I. Thus all CS plane orientations between (104) and (105) generate segments of (001) structure, four and five octahedra long; for orientations between (103) and (104), the segments are three and four octahedra long. Similarly, a second shear operation on an orientation close to (100) generates a stepped trace with all interfaces along (100). Recurrent crystallographic shear in both directions automatically cuts the parent ReO_3 structure into rectangular columns, as shown for the hypothetical generation of the *H*-Nb_2O_5 structure in Figure 21. Structures that have one CS plane direction in common can intergrow coherently on that plane; the second CS plane is kinked as it passes from one structure to the other. If, now, with one CS plane held constant, the other rotates, with concomitant change of composition, the relative proportions of the two types of {100} segment are altered, thereby changing the cross-sections of the blocks. This is illustrated in Figure 22 for structures with one common CS operation on $(601)_{ReO_3}$; a second CS operation on $(10\bar{4})_{ReO_3}$ generates $Nb_{25}O_{62}$ or, on $(20\bar{9})_{ReO_3}$, *H*-Nb_2O_5. If the CS surface remained planar, rotation between these two directions would give rise to regular intergrowth structures, with ordered, but in general complex, successions of steps in the CS plane. The simpler regular intergrowth sequences are known; the more complex sequences cannot be realized experimentally in a well ordered form, but have been found by electron microscopy as disordered intergrowths with kinked or wavy shear planes, corresponding to the out-of-equilibrium structures that have been observed in the simpler CS phases. Table 2 shows the relation between the parent ReO_3 structure and some block structure compounds; from the CS operator description follows the ability of different structures to generate intergrowth phases and to accommodate Wadsley defects through the kinking of CS planes.

The spacing between regularly recurrent CS planes prescribes the sizes of the columns enclosed between them. In the binary niobium oxides, block sizes smaller than (3 × 3) or larger than (3 × 5) octahedra—corresponding to normal distances 1.0—1.7 nm between CS planes—are not found, except as faults (*i.e.* as metastable configurations). Larger blocks, up to (5 × 5) and (3 × 6) octahedra, are found in the ternary WO_3–Nb_2O_5 and niobium oxyfluoride phases.[1] These limitations can be broadly understood in terms of Pauling's rules. The central octahedra in a block have the environment of the ReO_3 structure, little perturbed; an octahedron centred on a 5+ cation bears a net negative charge, which is balanced by a net positive charge on octahedra around the block corners. The whole structure can, in

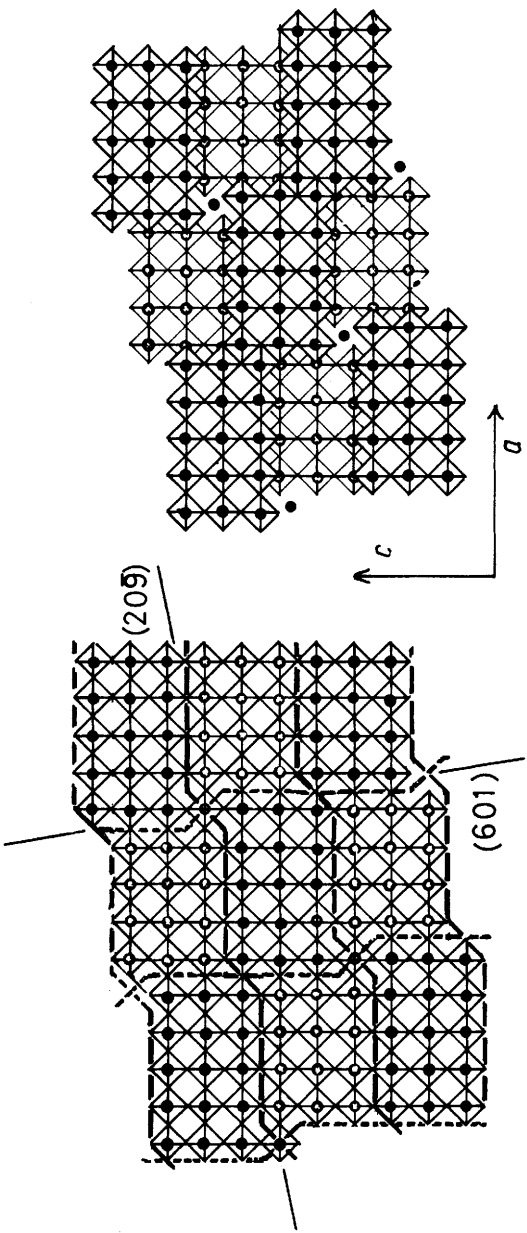

Figure 21 *Generation of the H-*Nb_2O_5 *structure by collapse of the basic* ReO_3 *structure along two CS planes,* (106) and (20$\bar{9}$). *Anion sites on the CS planes are eliminated; cation sites lying on the intersections of the CS operations move into tetrahedral co-ordination*

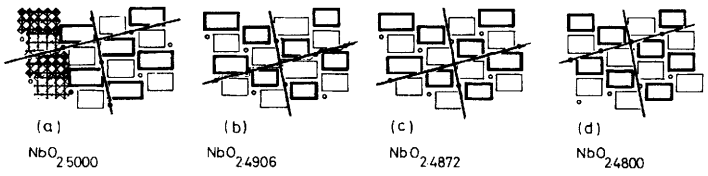

Figure 22 *Change of composition and generation of regular intergrowths as CS planes swing round in block structures*: (a) *H*-Nb_2O_5, *CS on* $(20\bar{9})$ *of parent* ReO_3 *structure* (*CS plane at* 12.53° *to* $(001)_{ReO_3}$); (b) 1 : 1 *intergrowth* $Nb_{53}O_{132}$, *CS on* $(40\bar{1}7)$ (13.24°); (c) 1 : 2 *intergrowth* $Nb_{39}O_{97}$, *CS on* $(50\bar{2}\bar{1})$(13.29°); (d) $Nb_{25}O_{62}$, *CS on* $(10\bar{4})$(14.04°). *The CS plane on* (601) *is common to all*

Table 2 *Generation of block structure types from* ReO_3 *structure by double crystallographic shear*

Compound	*Block structure*	*Generating crystallographic shear* $(\frac{1}{2}a)[\bar{1}10]/$	$(\frac{1}{2}a)[011]/$
$Ti_2Nb_2O_7$	$(3 \times 3)_\infty$	(100)	$(10\bar{3})$
$Nb_{12}O_{29}$	$(3 \times 4)_\infty$	(100)	$(10\bar{4})$
$Nb_{16}O_{40}$	$(4 \times 4)_\infty$	(100)	$(10\bar{4})$
$MgNb_{14}O_{35}F_2$	$(3 \times 5)_\infty$	(100)	$(10\bar{5})$
$Nb_{22}O_{54}$	$\{(3 \times 3)_1 + (3 \times 4)_\infty\}$	(601)	$(20\bar{7})$
$Nb_{47}O_{116}$	$\{(3 \times 3)_1 + (3 \times 4)_\infty\} + (3 \times 4)_2$	(601)	$(40\bar{1}\bar{5})$
$Nb_{25}O_{62}$	$(3 \times 4)_2$	(601)	$(10\bar{4})$
$Nb_{53}O_{132}$	$\{(3 \times 4)_1 + (3 \times 5)_\infty\} + (3 \times 4)_2$	(601)	$(40\bar{1}7)$
$Nb_{28}O_{70}$	$\{(3 \times 4)_1 + (3 \times 5)_\infty\}$	(601)	$(20\bar{9})$
$WNb_{12}O_{33}$	$(3 \times 4)_1$	(301)	$(10\bar{4})$
$W_3Nb_{14}O_{44}$	$(4 \times 4)_1$	(401)	$(10\bar{4})$
$W_5Nb_{16}O_{55}$	$(4 \times 5)_1$	(401)	$(10\bar{5})$
$W_8Nb_{18}O_{69}$	$(5 \times 5)_1$	(501)	$(10\bar{5})$

fact, be viewed as a packing of extended rod-like anionic and cationic elements, and would be destabilized by excessive charge separation. Thus the hypothetical $(6 \times 3)_\infty$ structure for Nb_2O_5, $Nb_{18}O_{45}$, appears to be outside the limits of stability, and has not been obtained. Detailed calculations of site potentials in block structures[43] modify the picture to some extent, but confirm that there are marked differences in site potential for cations within blocks and at corner and edge sites, which should lead to strong site-preference effects when ions of different charge are introduced. Larger blocks, with bigger elements of pure ReO_3 structure, can be formed only (*a*) if central cation sites can be occupied by ions of higher charge state, *e.g.* W^{6+}, or (*b*) if anion sites in central octahedra can be occupied by F^- or OH^- in place of O^{2-}. This accords with the observations. A redetermination of the crystal structures of $Ti_2Nb_{10}O_{29}$ and $TiNb_2O_7$ by neutron diffraction[44] has confirmed that there is indeed a strongly preferential occupation of corner

[43] A. K. Cheetham and R. Von Dreele, *Nature Phys. Sci.*, 1973, **244.** 139.
[44] A. K. Cheetham and R. Von Dreele, *Proc. Roy. Soc.*, in the press.

and edge sites by Ti^{4+} cations, the occupancy fractions conforming well to the sequence of calculated site potentials. This structure determination has also shown that the displacement vector of the crystallographic shear is not an exact lattice vector; the edge-shared octahedra are distorted so as to open out considerably the cation–cation distances at the interface, to the extent that the two close rows of cations can be just about resolved, in projection, in lattice images (see Figure 23).

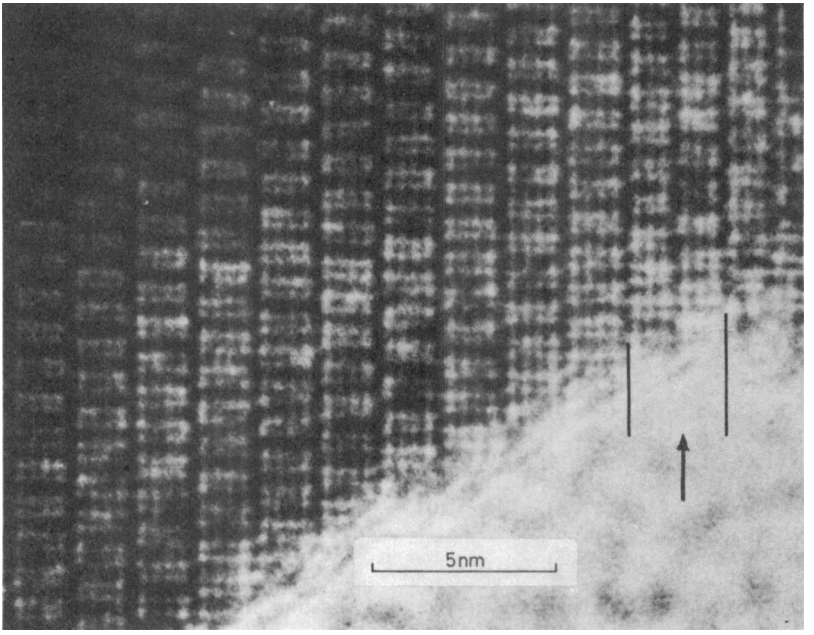

Figure 23 *Lattice image of the* $MgNb_{14}O_{35}F_2$ *phase in the system* MgF_2–Nb_2O_5 *with a Wadsley defect (arrowed) consisting of two rows of intergrown* $Mg_2Nb_{10}O_{25}F_4$ *structure*

Non-stoicheiometry and Defects in Block Structures.—As was made clear in the previous Report, lattice fringe imaging gave clear evidence that deviations from ideal stoicheiometry, and apparently bivariant thermodynamic behaviour of crystalline preparations, must be regarded as arising largely, if not entirely, from coherent intergrowth between two structures that were topologically compatible, but of different composition, *e.g.* $Nb_{25}O_{62}$ and *H*-Nb_2O_5, in the pseudo-bivariant range $NbO_{2.480}$—$NbO_{2.500}$.[33] Such intergrowths might be isolated lamellae one block wide (Wadsley defects) or more extended domains. The inferences drawn from relatively low-resolution electron microscopy have been fully confirmed by developments in high-resolution microscopy, which enable the $[NbO_6]$ octahedra to be counted

individually. Figure 23 shows in this way a defect with two rows of $M_{12}X_{29}$ structure intergrown in the $M_{15}X_{37}$ structure of $MgNb_{14}O_{35}F_2$.

The nature of thermal disorder in block structures has, as yet, received little attention, but Iijima[23] has recorded some suggestive observations on *H*-Nb_2O_5 quenched from the melt. For pure material, heated in air, the composition is necessarily $NbO_{2.5000}$. Nevertheless, in addition to domains of an alternative, metastable $(3\times3)_1$ block structure (crystallographic formula $Nb_{10}O_{25}$) which has also been obtained and characterized in a different way,[34] Iijima unambiguously identified lamellae of $(4 \times 3)_1$ blocks, *i.e.* of composition $Nb_{13}O_{33}$, $NbO_{2.538}$, which were in parts regularly spaced to form a long-period superstructure. Such oxygen-excess structure elements must be compensated by elements of some hypostoicheiometric structure, in equivalent amount. Compensating structural rearrangements, *e.g.* elements of $Nb_{25}O_{62}$ structure, were not always seen in association with these defects and the probable way in which a localized metal-excess can be incorporated is considered below. These observations do not relate to the statistical thermodynamic point-defect disorder, except to suggest that this is small, but are important as showing that local disorder transformations within a stoicheiometric crystal may involve adjustments of atomic positions, just as do the extrinsic faults already recognized, conforming always to the crystal chemical constraints of the block structures.

It is known that, in the complex polymorphism of Nb_2O_5,[45] crystallization in some of the metastable forms [*e.g.* the $(4 \times 4)_\infty$ structure of *N*-Nb_2O_5] is caused or promoted in the presence of certain dopants—fluorides, water (as source of OH^- anions), SnO_2, *etc.*—which are incorporated in very small amounts in the products. It is usually considered that dopant ions, of different charge from the host species that they replace, will be compensated by point defects: anion vacancies or interstitial cations would be needed to compensate the replacement of Nb^{5+} by Sn^{4+}. However, the doped niobium oxides have been found to grow with a domain structure, with regions of perfect structure separated by walls consisting of blocks of different size, and hence of different composition.[46] The anion : cation ratios in these domain walls, deduced from their block dimensions, indicate that they correspond to phases incorporating the dopant atoms. It would therefore appear that, at least in growth by vapour transport mechanisms, only restricted amounts of altervalent ions are incorporated, with compensating defects, in the structure of the product crystal. As growth proceeds from an adsorbed layer, the 'impurity' atoms are, from time to time, fully assimilated into elements of a new phase, with its own structure and composition, that can intergrow in perfect coherence with the main product. These observations have a bearing on more general problems of the mechanism of crystal growth—as, indeed, have many of the results emerging from lattice-imaging microscopy—and the facts could

[45] H. Schäfer, R. Gruehn, and F. Schulte, *Angew. Chem. Internat. Edn.*, 1966, **5**, 40; A. Reisman and F. Holtzberg, *J. Amer. Chem. Soc.*, 1959, **81**, 3182.

[46] J. S. Anderson, J. M. Browne, and J. L. Hutchison, *Nature*, 1972, **237**, 153.

in this case be detected and interpreted because of the peculiar suitability of block structures for study by lattice-imaging methods, but they may be indicative of the structural response of crystals to dopant atoms and have a wider significance.

Non-stoicheiometric Block Structures.—Reference was made in the last Report to the question whether certain of the block structure compounds have a genuine stoicheiometric range, or whether their apparent variability of composition could be accounted for entirely by the occurrence of Wadsley defects.

How far the apparent stoicheiometric existence ranges of block structures can be fully explained in terms of Wadsley defects is considered below. Systematic studies using chemical techniques and *X*-ray diffraction, such as those of Kimura[47] on the high-temperature thermodynamics of the NbO_2–Nb_2O_5 system, and of Gruehn[48] on the system Nb_2O_5–Nb_3O_7F, need to be supplemented by electron microscopy, but it is now possible to predict the types of Wadsley defect that may be expected. The approximate composition ranges found for phases in the oxyfluoride system are shown in Table 3. The basic structural components of these phases are the analogues of the oxides between $Nb_{25}O_{62}$ and *H*-Nb_2O_5, but involving blocks (3×5) and (3×6) in dimensions; one generating CS operation is on $(106)_{ReO_3}$, so that they can form coherent intergrowths with each other and with *H*-Nb_2O_5; the other CS plane swings round from $(50\bar{1})$ to $(60\bar{1})$. The existence ranges are then consistent with incorporation of Wadsley defects of structure III in *H*-Nb_2O_5, aperiodically and up to a substantial concentration. Beyond some limit, ordered domains of the regular 1 : 1 intergrowth structure II are formed. Phase III similarly should build in defects of structure I in its sub-stoicheiometric range [although, by analogy with the $(3 \times 4)_2$ structure of $Nb_{25}O_{62}$ a second mode of non-stoicheiometry is possible, as is discussed later]; Wadsley defects of structure V account for the excess-anion range. Similar considerations apply to the preparations with compositions between the limit of III and the ideal composition of V. Above that, between $NbX_{2.529}$ and $NbX_{2.532}$, extra rows of $(5 \times 3)_1$ structure are probably intergrown, even though the corresponding pure oxyfluoride, $Nb_{16}O_{39}F_2$, is not known; the isostructural $MoNb_{15}O_{40}F$ has been characterized. Both intergrowth phases II and IV appear as phases of fixed composition in *X*-ray diffraction; evidently where lamellae of two compatible structures are present in comparable, but irrational amounts, ordering processes maximize the size of domains of the simplest, regularly alternating sequence.

In a comprehensive summary of block structures, Gruehn[49] pointed out that careful chemical and *X*-ray-diffraction (Guinier camera) work indicated that those phases which had cations in tetrahedral sites, and only those,

[47] S. Kimura, *J. Solid State Chem.*, 1973, **6**, 438.
[48] R. Gruehn, *Z. anorg. Chem.*, 1973, **395**, 181.
[49] R. Gruehn, N.B.S. Special Publication 364, Solid State Chemistry, 1972, p. 63.

Table 3 *Apparent stoicheiometric ranges in niobium oxide fluoride structures*

	Phase	*Structure*	*Composition, x in* NbX_x		*Probable Wadsley defects*
			Ideal	*Observed*	
I	$Nb_{28}O_{70}$	$(3\times4)_1+(3\times5)_\infty$	2.5000	$2.500 \leqslant x \leqslant 2.504$	Structure III
II	$Nb_{59}O_{147}F$	$\{(3\times4)_1+(3\times5)_\infty\}+\{(3\times5)_2\}$ 1 : 1 intergrowth	2.5085	2.510	—
III	$Nb_{31}O_{77}F$	$(3\times5)_2$	2.5161	$2.515 \leqslant x < 2.520$	Structure I Structure V
IV	$Nb_{65}O_{161}F_3$	$\{(3\times5)_2\}+\{(3\times5)_1+(3\times6)_\infty\}$ 1 : 1 intergrowth	2.5231	2.523	—
V	$Nb_{34}O_{84}F_2$	$(3\times5)_1+(3\times6)_\infty$	2.5294	$2.526 < x < 2.535$	Structure III Structure VI
VI	$[Nb_{16}O_{39}F_2]$	$(3\times5)_1$	2.5625	Hypothetical	

showed well substantiated non-stoicheiometric behaviour; the 'ribbon' structures such as $Ti_2Nb_2O_7$, $(3 \times 3)_\infty$, and $Nb_{12}O_{29}$, $(3 \times 4)_\infty$, were of ideal, invariable composition in monophasic preparations. For example, $TiNb_{24}O_{62}$ and $Nb_{25}O_{62}$ appear to have a range of composition on the metal-rich side (Table 4) which does not include the ideal composition; preparations with the exact composition $M_{25}O_{62}$ ($MO_{2.480}$) are invariably biphasic in *X*-ray diffraction. Although coherently intergrown single strips or narrow lamellar domains of a second structure would not be detected by *X*-ray methods, the distinction between compounds with and without tetrahedral sites supports the contention that the observations are genuine. Further evidence, from electron-microscope study of local structure, comes from the work of Allpress and Roth[50] on the Nb_2O_5–WO_3 system. $WNb_{12}O_{33}$ $[(3 \times 4)_1]$ and *H*-Nb_2O_5 $[(3 \times 4)_1 + (3 \times 5)_\infty]$ can both intergrow coherently and form a succession of regular intergrowth phases. An excess of cations, above the ideal formula $MO_{2.5385}$, could therefore be accommodated by intergrowing occasional Wadsley defects with the *H*-Nb_2O_5 structure. A thorough study of the system showed, however, that such Wadsley defects were not present in well annealed preparations between the ideal composition $WO_3,6Nb_2O_5$ and a limit of $WO_3,8Nb_2O_5$. If it is tentatively accepted that the anion sublattice provides the framework for the block structures, this limiting composition could be expressed as $M_{13.05}O_{33}$, with $(3 \times 4)_1$ blocks, as observed, but with a cation excess incorporated in some way.

In addition to this evidence for variability of composition, there are a few compounds for which it is impossible to reconcile the chemical composition with the block structure, as determined, without invoking some form of defect to accommodate a cation excess. One such is a phase to which Levin[51] ascribed the composition $GeO_2,9Nb_2O_5$, which appears to be isostructural with PNb_9O_{25}, a $(3 \times 3)_1$ block structure. A second is a phase with a narrow composition range around $P_2O_5,22Nb_2O_5$ but necessarily with the total stoicheiometry $MO_{2.5000}$;[52] Allpress reported this as having the structure $\{(3 \times 3)_1 + (3 \times 4)_1\}$, corresponding to the ideal formula $M_{23}O_{58}$, again with a cation excess if the real unit-cell composition is expressed as $M_{23.2}O_{58}$. A determination of the structure for such unambiguous cases of metal-excess defect structures would probably furnish a key to the problem of non-stoicheiometric block structures just discussed.

The structure of '$GeO_2,9Nb_2O_5$' has now been determined by both neutron-diffraction and *X*-ray-diffraction methods.[32] The scattering factors for germanium and niobium differ in opposite senses for neutrons and for electrons; neutron diffraction is particularly suited for determining the occupation fractions of oxygen sites, since the scattering lengths of all the atoms in the crystal are comparable in magnitude. Accepting Levin's composition for the compound, extreme possibilities would be that the

[50] J. G. Allpress and R. S. Roth, *J. Solid State Chem.*, 1971, **3**, 209.
[51] E. M. Levin, *J. Res. Nat. Bur. Stand., Sect. A*, 1966, **70**, 5.
[52] E. M. Levin and R. S. Roth, *J. Solid State Chem.*, 1970, **2**, 250.

Table 4 *Composition ranges reported for block-structure oxides with tetrahedral sites occupied*

Oxide	O : M *Ratio* *Ideal*	*Observed limits*	*Composition for perfect column structure*	*Maximum occupancy number for tunnel sites*
$WNb_{12}O_{33}$	2.5385	2.529—2.538	$M_{13.05}O_{33}$	1.05
$Nb_{28}O_{70}$	2.5000	2.490 or 2.495 —2.500	$M_{28.12}O_{70}$ or $M_{28.06}O_{70}$	1.12—1.06
$TiNb_{52}O_{132}$ / $Nb_{53}O_{132}$	2.4906	2.483	$M_{53.16}O_{132}$	1.08
$TiNb_{24}O_{62}$ / $Nb_{25}O_{62}$	2.4800	2.472—2.478	$M_{25.08}O_{62}$— $M_{25.02}O_{62}$	1.08—1.02
$Nb_{47}O_{116}$	2.4681	2.460	$M_{47.15}O_{116}$	1.075
		2.464—2.467	$M_{47.08}O_{116}$— $M_{47.02}O_{116}$	1.04—1.01
$Nb_{22}O_{54}$	2.4545	2.453	$M_{22.014}O_{54}$	1.01
'GeO_2,$9Nb_2O_5$'	2.5000	2.474	$M_{10.11}O_{25}$	1.11
'P_2O_5,$22Nb_2O_5$'	2.521	2.5000 (10)	$M_{23.20}O_{58}$	1.06

unit-cell composition would be $M_{10}O_{24.74}$ if the cation sublattice were perfect, or $M_{10.11}O_{25}$ if the oxygen sublattice were perfect. There must be either oxygen 'vacancies' or metal 'interstitials', or both. From the highly concordant structure determinations it emerged (*a*) that, within narrow error limits, all oxygen sites were fully occupied and (*b*) that all the octahedral cation sites within the blocks were fully occupied, and occupied by niobium atoms. It follows that the main structure of the crystal, provided by the interfaced columns of $[NbO_6]$ octahedra, is essentially perfect; the formula can be written as $(Nb,Ge)_{1.11}(Nb_9O_{25})$, with the cation excess wholly associated with the way in which possible cation sites are occupied in the channels formed by the corners of the columns (Figure 24). It is reasonable inference that this principle is more widely applicable to the problem discussed in the beginning of this section. The structure determinations showed, in addition, that not all the cations in the channels were on tetrahedral sites but also occupied sites in the corners of the channels which, as close examination of the structure shows, places them in octahedral co-ordination, as outlying appendages to the square columns (Figure 24b). Such potential octahedral sites occur in pairs, at each level $z = 0$, $z = \frac{1}{2}$, and although the insertion of a pair of cations in these sites inevitably blocks the occupation of one tetrahedral site, it provides a means of 'over-filling' the channels. This clearly occurs, to the extent of about 10%. The problem is why it does not proceed further, up to the structurally limited end-composition $M_{11}O_{25}$, corresponding to complete occupation of octahedral sites and elimination of tetrahedral cations. 'GeO_2,$9Nb_2O_5$' may have a narrow composition range on the Nb_2O_5-rich side (virtually a solid solution with $Nb_{10}O_{25}$, as is the case for PNb_9O_{25}), but the GeO_2-rich limit is certainly close to the composition assigned by Levin. Several reasons for the restriction on octahedral site occupancy could be advanced: (*a*) that interactions between cations in the channels impose a one-dimensional ordering, as illustrated in Figure 24g; (*b*) that the distribution of octahedral and tetrahedral sites is linearly randomized, and determined by the statistical thermodynamics of site preference; (*c*) that the constraint is thermodynamic, and imposed by coexistence with GeO_2 as a separate phase. If the arrangement is ordered, there is evidently little or no correlation between any one channel and its neighbours, since there is no trace of superlattice ordering. This conclusion would be significant for defect tunnel structures in a wider context.

If this solution of one defect structure can be regarded as typical, and extended to the non-stoicheiometric behaviour considered earlier, it would appear that all the facts fit a consistent pattern, with the channels of tetrahedral sites stuffed to a maximum excess of 5—10% (*cf.* Table 4, columns 5 and 6). That the $M_{25}O_{62}$ structures cannot attain the ideal composition would indicate that the site preference energies are rather finely balanced. Iijima's observations on melt-quenched *H*-Nb_2O_5 also fall into place. The type of disorder found—whether thermal intrinsic disorder or metastable disorder, frozen into the sample—showed a local reorganization that pro-

vided an excess of $(4 \times 3)_1$ blocks. If the associated corner channels had only their normal complement of cations in tetrahedral sites, there would have been oxygen-excess structure elements, $Nb_{13}O_{33}$; with the total composition of the crystal fixed as $NbO_{2.5000}$, it is likely that the compensating defects were 'stuffed' channels, with octahedral sites occupied.

There is, however, some evidence that the interpretation of these phenomena is not yet complete, from Kimura's investigation[47] of the thermodynamics of the NbO_x ($2 \leqslant x \leqslant 2.500$) system at 1300 and 1400 °C. In each experiment, the equilibration with gas buffer mixtures was approached from both sides: by oxidation of NbO_2 and by reduction of Nb_2O_5. Under

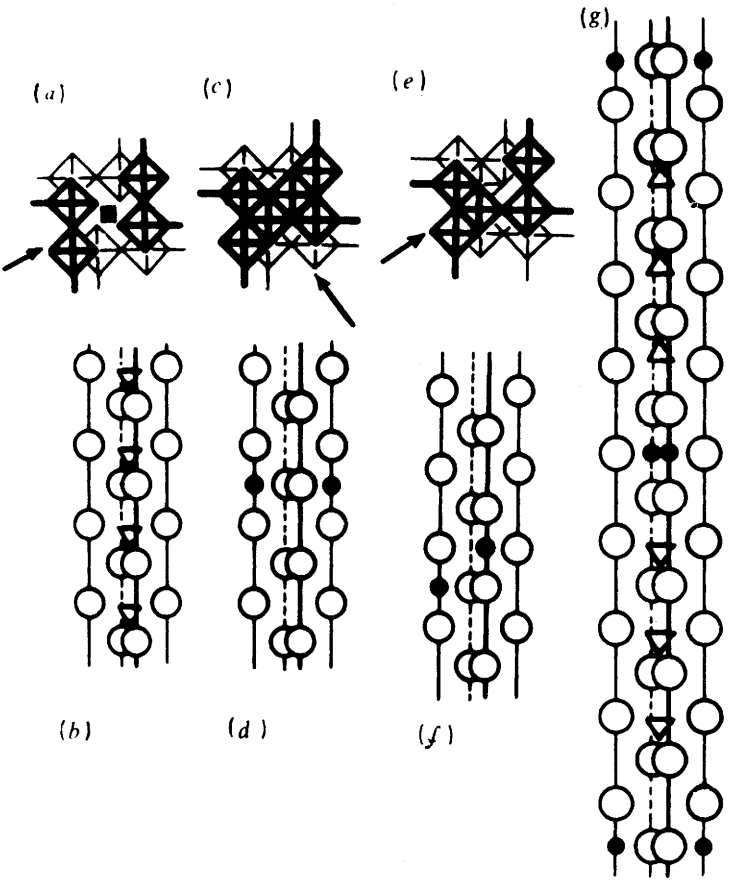

Figure 24 (a), (b): *plan and b-axis projection of normal tetrahedral cation environment at block corners;* (c), (d) *and* (e), (f): *insertions of cations in octahedral co-ordination, replacing tetrahedral sites;* (g): *the possible ordered sequence of tetrahedral and octahedral cations in the corner channels in* $GeO_2{,}9Nb_2O_5$

these conditions there can be fair confidence that an equilibrium composition and, hopefully, an equilibrium structure, was reached, and on this basis Kimura attempted a thermodynamic analysis in terms of the concentration of four distinguishable types of oxygen atom: those in the block interiors, linked to two six-co-ordinate Nb cations; those in the block edges, co-ordinated to three six-co-ordinate Nb; those at the block corners, with four six-co-ordinate Nb; and those that build up the channels of tetrahedral sites, each linked to one octahedral and one tetrahedral cation. Oxidation and reduction processes were then treated in terms of changes in the concentration of each of these species, the crystal as a whole being regarded as a regular solution system. On this basis, equilibrium constants for the partial reactions governing the concentrations of the different types of oxygen could be derived, and these accounted well not only for the observed ranges of existence of the phases observed between (and including) the $Nb_{22}O_{54}$ and H-Nb_2O_5 structures, but also for the noteworthy fact that the upper limiting compositions of $Nb_{22}O_{54}$, $Nb_{47}O_{116}$, $Nb_{25}O_{62}$, and $Nb_{53}O_{132}$ all lie on the metal-rich side of the theoretical composition. Kimura's conclusion is that the equilibrium configuration corresponds to the dispersion of localized defects, and that Wadsley defects are not the predominant form of accommodating non-stoicheiometry. His treatment does not take account of the 'tunnel stuffing' that has been established by structure determinations for $(Nb,Ge)_{10.11}O_{25}$, but it is clear that the problem of defects in block and CS structures can only be resolved by electron microscopy of the local structure. Reports on this have not yet appeared, but it is of interest that Iijima[53] has obtained evidence for the presence of localized defects—relaxed defect complexes rather than classical point defects—in Kimura's materials.

The essence of this and related solid-state problems is that the linked changes of composition and structure fall into a category of partially reconstructive transformation. Non-reconstructive (*e.g.* martensitic) transformations are kinetically unhindered; once initiated, they go to completion. Fully reconstructive transformations depend upon a large fluctuation that nucleates a new configuration; a reaction interface moves through the solid, transferring atoms from one structure to the new equilibrium structure of the product. Between these is the situation in which a composition change can be accommodated in several ways, none of which requires radical shifts in the positions of the atoms, for example by rotation of CS planes, by lateral migration of CS planes to alter the spacing between them, or by creation of localized defects within the elements of parent structure, with or without change in the orientation and spacing of CS planes. The total lattice energy may differ little for alternative configurations, but the kinetics of the processes involved may be different. Under these circumstances, the observed chemistry and structure of a system may, in reality, be explored over a metastable free energy surface in temperature–composition–chemical potential space.

[53] S. Iijima, personal communication; to be published.

5 Infinitely Adaptive Structures

From the phenomenon of pivoting CS planes, discussed in a previous section, and from observations of the superlattice ordering in certain structures, considered below, emerges the concept that, in certain structure types, a fully ordered structure may be formed for every possible composition.[54] Changes in the total atomic ratios of a solid-state system (within a certain range) do not then result in separation into two coexisting phases, neither do they involve the randomized introduction of defects, as in typical non-stoicheiometric solid-solution systems. Instead, the structure adapts its long-range order to define a new crystallographic repeating unit, maintaining a common structural principle.

CS Phases.—It will be clear that the composition of a CS phase can be altered in two ways: by change in the width of the slab of parent structure between CS planes of a given orientation, or by change of orientation of CS planes enclosing slabs of essentially constant width. The former change takes place in discrete steps, generating a homologous series for every CS plane orientation; the latter is, or can be, a continuous process. These two modes are quite independent as regards attainment of order. Variable spacing between CS planes—implying a non-equilibrium departure from fixed stoicheiometry—is frequently found when the lateral spacing (and hence the interaction) between CS planes is large, but observations on rutile- and ReO_3-type CS phases leave no doubt that the equilibrium configuration of any CS surface is planar. This implies that the APB and CS segments in the CS plane take up a regular, repeating sequence.

Considering, for simplicity, CS phases derived from the ReO_3 structure, a compound M_nO_{3n-m} is formed by the omission of every nth $(hk0)$ sheet of anion sites, where m depends upon the CS plane orientation $(hk0)$. The normal spacing between CS planes, d_{CS} is related to n by

$$d_{CS} = d_{hk0}(n - c), \qquad (c = \text{fractional collapse})$$

so that the homologous series (n variable) can be represented by a set of composition points on a nearly linear plot of composition against d^*_{CS} $(= 1/d_{CS})$ (Figure 25). A similar array of composition points could be plotted for every orientation; as has been seen, there is a continuum of possibilities. If, now, the orientation be written as $(h'10)$, where $h' = h/k$, the transverse lines with n = constant represent paths by which the crystal could change its composition without introducing or eliminating CS planes. As long as the sequence of segments in the CS planes adjusts itself to a regular repeating pattern, the system remains fully ordered.

[54] J. S. Anderson, *J. C. S. Dalton*, 1973, 1107.

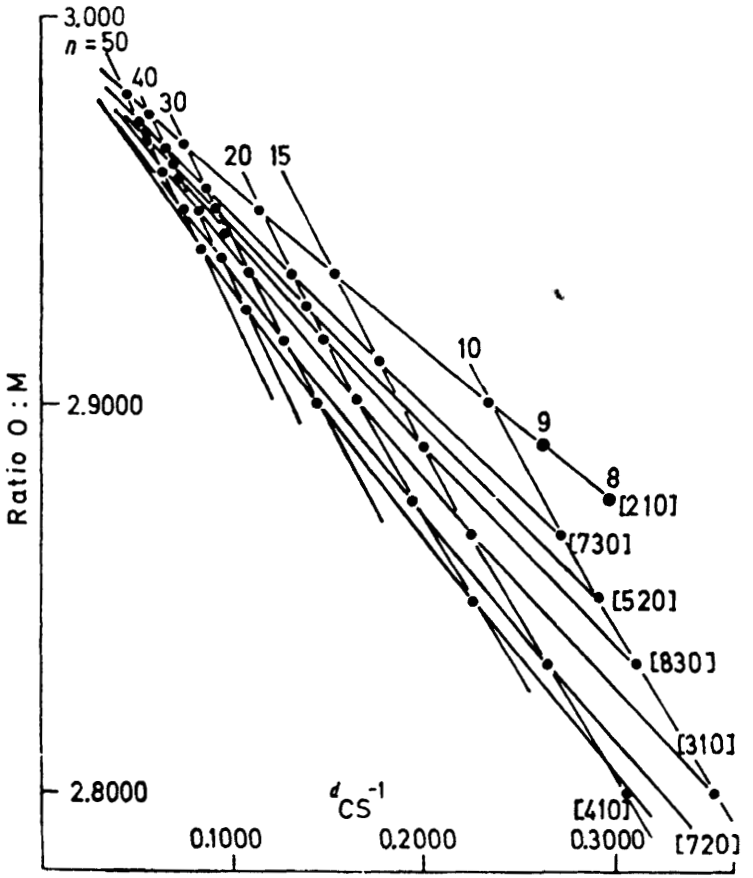

Figure 25 *Change of composition and reciprocal of the spacing between CS planes in* ReO_3*-based structures as the CS plane swings round from* (410) *to* (210)

Adaptive Superlattice Ordering.—A somewhat different, but related, situation is found in certain structures in which a one-dimensional ordering process generates a superlattice from a simpler sub-cell. The occurrence of adaptive ordering in such a system—the low-temperature polymorph of Ta_2O_5—was established experimentally by Roth and Stephenson[55] before the full implications were recognized. *L*-Ta_2O_5 and ternary oxides derived from it have structures related to that of U_3O_8, basically consisting of ribbons of edge-sharing pentagonal-bipyramidal [MO_7] co-ordination groups extending along one crystallographic direction (the *b* axis). The metal atoms form a pseudo-hexagonal (orthorhombic) array, but the oxygen atom positions and small

[55] R. S. Roth and N. C. Stephenson, 'The Chemistry of Extended Defects in Non-metallic Solids', ed. L. Eyring and M. O'Keefe, North-Holland, Amsterdam, 1970, p. 167.

displacements of the metal atoms impose a superstructure of this pseudo-hexagonal subcell, along the *b* direction. WO_3, ZrO_2, Al_2O_3, and other oxides simulate the formation of solid solutions with L-Ta_2O_5,[56] but careful X-ray-diffraction study reveals that the superstructure lines display a remarkable behaviour. They shift systematically and continuously with changes of composition. Each one of a wide range of compositions between Ta_2O_5 and $4WO_3{,}11Ta_2O_5$, examined by single-crystal X-ray methods, had a unique superstructure; in no well annealed specimen were two phases, each with its own superstructure, found to coexist in equilibrium.[57] It was necessary to assign high values to the superstructure multiplicity.

The interpretation of these facts, based on single-crystal structure determinations[58] and the related structure of U_3O_8,[59] is that the superstructure arises from the folding or undulation of the ribbons of pentagonal bipyramids, with a periodicity commensurable with a repeating unit of 5, 8, 11 ... $3n + 2$ subcell spacings along the *b* axis (Figure 26). This generates a set of homologous subunits $M_{10}O_{26}$, $M_{16}O_{42}$, $M_{22}O_{58}$ ... $M_{2n}O_{(16n-2)/3}$. These subunits may themselves be stacked along the *b* axis, in varying proportions but in a repeating sequence, to form a longer superlattice. Denoting the multiplicities of the subunits by m_1, m_2 ... m_i, and the number of each in the true superlattice repeat by a_1, a_2 ... a_i, the total multiplicity m^* may be written as

$$m^* = a_1m_1 + a_2m_2 + \cdots = \sum a_im_i$$

If the compositions of the subunits are denoted by x_1, x_2 ... x_i, the composition of the true repeating unit is $x^* = \sum a_ix_i$. Changes of composition in the phases formed between a pair of oxides (*e.g.* WO_3 and Ta_2O_5) imply changes in chemical potential, and it would appear that these impose the thermodynamic constraint (analogous to the biphasic equilibrium between compounds in an ordinary pseudobinary system) that only adjacent pairs of subunits can exist within any one structure. By changes in the relative proportions of subunits, every possible composition between $M_{10}O_{26}$ and $M_{16}O_{42}$, $M_{16}O_{42}$ and $M_{22}O_{58}$, *etc.* could form, in principle, an ordered structure, with the multiplicities $m^* = 5a_1 + 8a_2$, or $8a_2 + 11a_3$, *etc.* Figure 27 shows the hypothetically continuous variation of composition as the ratio $a_1 : a_2$, $a_2 : a_3$ changes, together with the compositions actually examined and the superstructure multiplicities assigned by Roth and Stephenson.

This is the structural principle. The actual situation in the L-Ta_2O_5 oxide series is rather more complex in that the oxygen : metal ratios, running from 2.49 in Al_2O_3– and ZrO_2–Ta_2O_5 phases to 2.5769 in $WTa_{22}O_{67}$, are all oxygen deficient as compared with the ideal structures (ratio = 2.6000, 2.6250, and 2.6364 for $m = 5$, 8, and 11 respectively). In the real structures,

[56] R. S. Roth and J. L. Waring, *J. Res. Nat. Bur. Stand., Sect. A*, 1970, **74**, 485.
[57] R. S. Roth, J. L. Waring, and H. S. Parker, *J. Solid State Chem.*, 1970, **2**, 445.
[58] N. C. Stephenson and R. S. Roth, *Acta Cryst.*, 1971, **B27**, 1010, 1018, 1025, 1031, 1037.
[59] A. S. Andreasen, *Acta Cryst.*, 1958, **11**, 612; B. O. Loopstra, *ibid.*, 1964, **17**, 651.

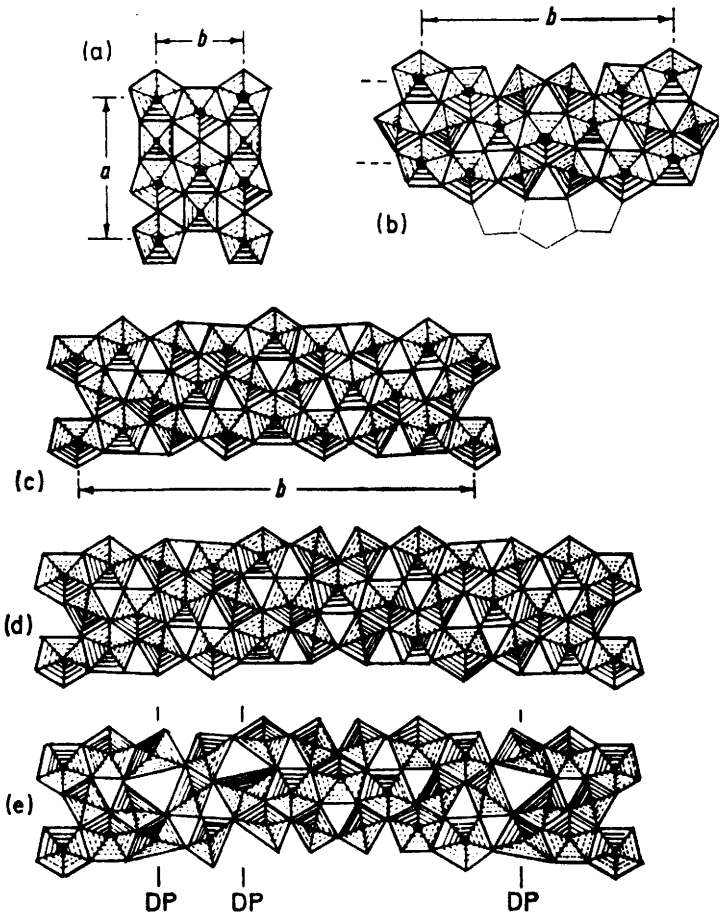

Figure 26 *Structural principle of L-*Ta_2O_5 *and related compounds*: (a) U_3O_8; (b) $m = 5$ *unit*, $M_{10}O_{16}$, *showing folding of the chain of pentagonal bipyramids*; (c) $m = 8$ *unit*, $M_{16}O_{42}$; (d) $m = 11$ *unit*, $M_{22}O_{58}$; (e) Ta_2O_5, $Ta_{22}O_{55}$ *with three distortion planes* (*DP*) *per unit cell*

as illustrated in Figure 26e for the $m^* = 11$ form of Ta_2O_5 itself, some oxygen sites are periodically eliminated, leaving the metal atoms in highly distorted co-ordination polyhedra. Such distortion planes could be introduced, singly or in pairs, at every folding point of the undulating chains of pentagonal bipyramids. A maximum is thereby set to the number of oxygen atoms that can be omitted from each basic subunit, and from each superstructure multiplicity m^* there could, in principle, be derived a homologous series of compounds, with discrete compositions arising from the operation of a

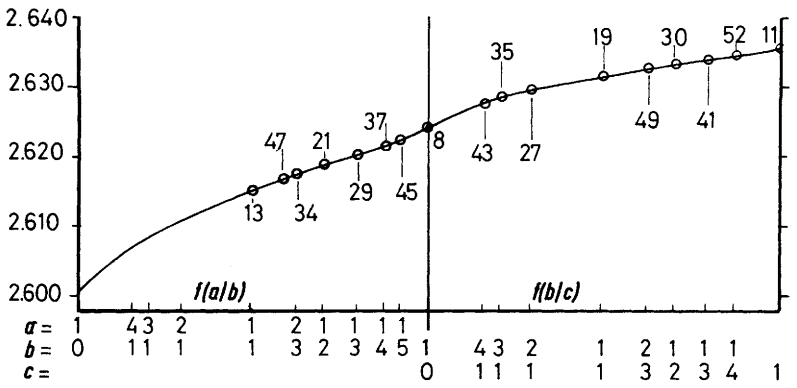

Figure 27 *Change of composition in (filled) L-*Ta_2O_5*-like structures as the ratio of constituent subunits changes. Marked points show total superstructure multiplicities identified in* Ta_2O_5–WO_3 *series of phases*

variable number p of distortion planes per true unit cell, where $0 \leqslant p \leqslant p_{max}$. The general formula for such compounds could be expressed as

$$M_{2m^*}O_{\{2(8m^*-a_1-a_2)/3\}-p}$$

If the linear density of distortion planes (*i.e.* d^*_{DP}) is taken as a configurational parameter and plotted against the composition, every multiplicity m^* generates a linear array of composition points. Figure 28 shows this for some of the m^* values identified by Roth and Stephenson. If long-range ordering is indeed capable of arranging the subunits into indefinitely large superstructures, the arrays of composition points form a continuum, and a second mechanism is provided whereby a solid solution or mixed-valence phase could vary continuously in composition without any disorder.

In any particular system (*e.g.* the Ta_2O_5–WO_3 system as shown in Figure 28, and similarly for phases reported in the Al_2O_3–Ta_2O_5 system,[58] and for a particular temperature of internal equilibration, there is clearly some superstructure sequence and density of distortion planes that represents the most stable configuration, but each composition does not necessarily correspond to a unique structure. In particular, the composition $MO_{2.5000}$ is represented by a composition point for every possible value of m^*—an infinity of potential superlattice structures. There is indeed direct evidence from the crystallographic literature,[60] and from newer electron-microscopic work, that the superlattice of *L*-Ta_2O_5 changes with the temperature of annealing; the value $m^* = 11$ and structure found by Roth and Stephenson relate specifically to the oxide as equilibrated at *ca.* 1200 °C.

A related situation is found in the 'solid solutions' formed in the YOF–

[60] *E.g.* R. Moser, *Schweitz. mineral petrograph. Mitt.*, 1965, **45**, 35.

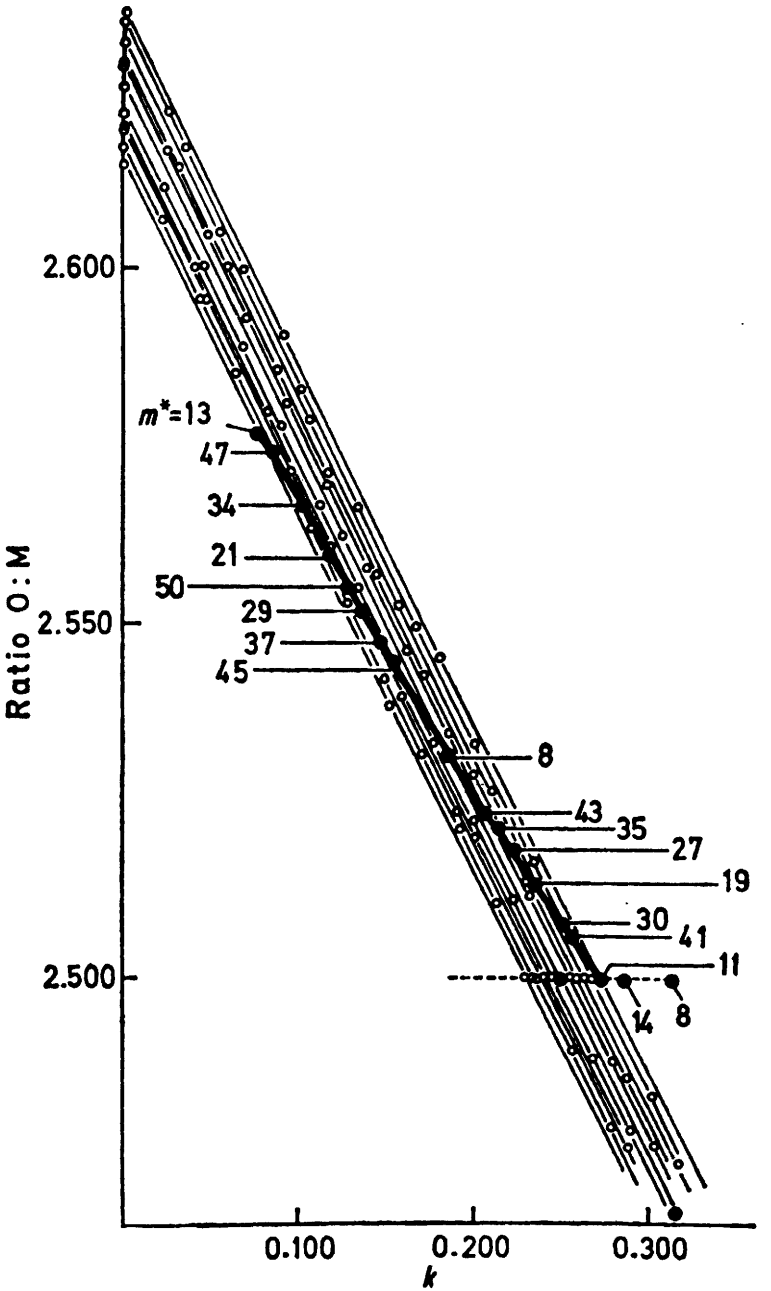

Figure 28 *L*-Ta_2O_5 *superstructures: variation in composition with reciprocal of average position between distortion planes for several observed multiplicities m*. Points represent compositions, for each m* value, as successive distortion planes are introduced. The heavy line joins composition points identified in the* Ta_2O_5–WO_3 *system*

YF_3 [61] and the zirconia-rich ZrO_2–Nb_2O_5 [62] systems, which provide a one-dimensionally ordered means of accommodating an anion excess in structures related to the fluorite type. Bevan and Mann have interpreted the former in terms of regularly recurrent layers in which all the excess of anions is concentrated, and having a structure related to that of YF_3, interpolated along one axial direction of the (distorted) fluorite structure of YOF. If such a 'stuffed' layer recurs every n fluorite cells, the composition of the ordered structures is $Y_nO_{n-1}F_{n+2}$. Over the composition range $YX_{2.130}$—$YX_{2.220}$ (X = O + F), however, careful *X*-ray-diffraction work shows the characteristic behaviour already mentioned: the superstructure lines shift continuously with composition; no two compositions, however closely spaced and however irrational, had the same superstructure, neither did any show any splitting of superstructure lines, indicative of two ordered phases coexisting; the observed superstructure lines could, for most preparations, be interpreted only in terms of high multiplicities. These high multiplicities could be interpreted as arising from the regularly recurrent sequence of a set of subunits with individual multiplicities $n = 4, 5, \ldots 8$. The total superstructure multiplicity m^* is then given by $m^* = a_1n_1 + a_2n_2$ and the corresponding composition, $Y_{m^*}X_{2m^*+a_1+a_2}$, can be symbolized $(n_1)_{a_1}(n_2)_{a_2}$. Data for the closely spaced compositions examined by Bevan and Mann are shown in Table 5.

Table 5 *Closely spaced superstructure phases in* $Y(O,F)_n$

Composition n (experimental)*	*Assigned multiplicity*	*Constitution*	*C-axis/* Å	*Composition n (calculated for structure)*
2.13(6)	23	$(8)_2(7)_1$	126.7	2.130
2.11(5)	7	$(7)_1$	38.6	2.143
2.14(8)	19	$(7)_1(6)_2$	104.9	2.153
2.14(9)	45	$(7)_3(6)_4$	248.2	2.155
2.16(5)	6	$(6)_1$	33.1	2.167
2.17(1)	17	$(6)_2(5)_1$	94.0	2.176
2.18(3)	47	$(6)_2(5)_7$	260.0	2.191
2.18(7)	57	$(6)_2(5)_9$	315.4	2.193
2.22(0)	28	$(5)_4(4)_2$	155.2	2.214
2.25(9)	41	$(5)_5(4)_4$	227.4	2.220

* Fourth, bracketed digit uncertain in significance.

For these structures, the composition uniquely determines the mode of ordering. There is no mechanism whereby a given super-superstructure can generate a family of homologous compounds. In this respect the situation is clearer, and the interpretation more direct, than for the *L*-Ta_2O_5 phases.

The experimental observations hardly permit any other interpretation that that certain phases have what may be termed infinitely adaptive structures.

[61] D. J. M. Bevan, ref. 49, p. 479; A. W. Mann and D. J. M. Bevan, *J. Solid State Chem.*, 1972, **5**, 410.

[62] J. L. Galy and R. S. Roth, *J. Solid State Chem.*, 1973, **7**, 277; R. S. Roth, J. L. Waring, W. S. Brouwer, and H. S. Parker, ref. 49, p. 183.

The question of how far a crystal can really adjust its structure to its composition, to exhibit a continuum of ordered structures, has to be considered at two levels. At the philosophical level, the problem is that of attaining long-range order with large repeating units of structure. In the cases cited, the repeating units are up to a few hundred ångströms in length and the nature of the interactions that impose such large repeat patterns is not well understood. It is evident that, as the superlattice dimensions increase, the energetic difference between a perfectly ordered structure and one with mistakes in stacking, or in the sequence of APB and CS steps in a crystallographic shear plane, must become smaller than the activation energy for the requisite rearrangement process. A genuine continuum of perfect structures must be unattainable. Operationally, it is not possible to characterize the ordered structures with sufficient precision to discriminate between very closely spaced ratios of the subunits that determine the stacking multiplicity or the orientation of CS planes. It will be noted that, for *L*-Ta_2O_5, Roth and Stephenson limited their superstructure assignments to values around or below 50, corresponding to small values for the proportions of the constituent subunits. Similarly, for the Cr_2O_3–TiO_2 CS phases, Bursill, Hyde, and Philp rationalized the orientations of the CS planes to fairly small values for h, k, and l. The precision attainable in measuring the positions of *X*-ray- and electron-diffraction spots does not permit any other course. In Table 5, the discrepancies between the composition of the material and that calculated from the structure illustrate the problem; for the particular crystals examined, there is little doubt that the calculated compositions are the more reliable.

Although, therefore, real systems must approximate, rather than conform exactly, to the concept of infinitely adaptive structures, the consequences need to be worked out in their bearing on the nature and thermodynamics of solid solution systems, broadly interpreted. The role of ordering processes has become apparent in relation to a rather exceptional group of materials, which exhibit the requisite internal mobility and unspecified long-range interactions. There are other solid systems to which the same considerations may well apply, which are known (for example) to exhibit variable and irrational superlattice ordering, suggestive of a large true repeating unit. The variable-composition $Fe_{1-x}S$ phase now appears to be of this type.[63] Problems of this kind merit careful study; mobile, adaptive superstructure ordering could well have a wider bearing on highly defective solid-solution phases and non-stoicheiometric compounds.

[63] N. Morimoto, H. Nakazawa, K. Nishiguchi, and M. Tokonami, *Science*, 1970, **168**, 964; H. Nakazawa and N. Morimoto, *Materials Res. Bull.*, 1971, **6**, 345.